Zero-temperature thermodynamics of dense asymmetric strong-interaction matter

Jens Braun[1,2] and Benedikt Schallmo[1]

[1]*Institut für Kernphysik, Technische Universität Darmstadt, D-64289 Darmstadt, Germany*
[2]*ExtreMe Matter Institute EMMI, GSI, Planckstraße 1, D-64291 Darmstadt, Germany*

(Received 29 June 2022; accepted 14 September 2022; published 21 October 2022)

Employing constraints derived from the microscopic theory of the strong interaction, we estimate the zero-temperature phase structure of dense isospin-asymmetric matter with two quark flavors. We find indications that strong-interaction matter along trajectories relevant for astrophysical applications undergoes a first-order phase transition from a color-superconducting phase to an ungapped quark-matter phase when the density is increased. Such a phase transition is found to be absent in isospin-symmetric matter. Moreover, by taking into account constraints from β equilibrium, charge neutrality, and color neutrality, we provide an estimate for the speed of sound in neutron-star matter. Notably, we observe that the speed of sound in neutron-star matter exceeds the asymptotic value associated with the noninteracting quark gas and even increases toward lower densities across a wide range, in agreement with recent results for isospin-symmetric matter. Considering results from studies based on chiral effective field theory at low densities, our findings suggest the existence of a maximum in the speed of sound for $n/n_0 \lesssim 10$, where n_0 is the nuclear saturation density.

DOI: 10.1103/PhysRevD.106.076010

I. INTRODUCTION

The detection of the gravitational-wave signal of a neutron-star merger [1,2], the ongoing missions aiming at direct neutron-star radius measurements [3–8], and precise mass measurements of heavy neutron stars [9–12] put our understanding of the dynamics of dense matter to the test; see Ref. [13] for a recent discussion. In fact, a quantitative theoretical description of astrophysical objects requires a detailed knowledge of the equation of state (EOS) of strong-interaction matter over a wide range of densities, up to ten times the nuclear saturation density (or maybe even higher). In addition, for the description of neutron-star mergers, information on the temperature dependence of the EOS (up to temperatures of $\sim$100 MeV) may also become very relevant. Unfortunately, the theoretical description of strong-interaction matter across a wide density and temperature range is highly nontrivial, as it requires us to bridge the gap between different (effective) degrees of freedom.

At low densities, chiral effective field theory (EFT) provides a framework to describe the properties of nuclear matter in a systematic fashion by means of pions and nucleons as low-energy degrees of freedom [14]. As a consequence, calculations based on chiral EFT interactions yield strong constraints for the low-density part of the EOS [15,16]; see Ref. [17] for a review. For related functional renormalization group (fRG) studies, we refer the reader to Refs. [18–24].

Going beyond the nucleonic low-density regime, the situation is less clear with respect to the dominant effective degrees of freedom. In fact, an analysis of the renormalization group (RG) flow of gluon-induced four-quark interaction channels in a Fierz-complete setting for two massless quark flavors suggests that many interaction channels (including vector channels) become equally strong in a range of densities close to the nucleonic low-density regime [16]. A quantitative description of the dynamics in this regime therefore requires us to include at least vector channels, as also discussed in Refs. [25–27]. In fact, the inclusion of such channels may even lead to a qualitative change of the EOS in this density regime [26].

Increasing the density even further, the aforementioned Fierz-complete study of gluon-induced four-quark interaction channels suggests the formation of a chirally symmetric diquark condensate associated with pairing of the two-flavor color-superconductor (2SC) type, as indicated by a clear dominance of the corresponding four-quark channel [28]. This channel has also been considered in various early seminal works, ranging from low-energy model studies [29–32] to first-principles studies relying on the fact that the strong coupling becomes small at high densities, owing to asymptotic freedom [33–39]. Given this plethora of studies, it is presently indeed widely accepted that strong-interaction matter at low temperatures and sufficiently high densities is a color superconductor with diquarks as effective degrees of freedom; see Refs. [40–51] for reviews. Finally, at very high densities and under the assumption that a potentially existing color-superconducting gap in the excitation spectrum of the quarks is small compared to the chemical potential, constraints on the EOS have been computed in a perturbative setting [52–60].

The "detection" of the most relevant effective degrees of freedom in certain density ranges is very relevant for astrophysical applications since it opens up the opportunity to provide reliable constraints on the EOS of QCD over a wide density range. Indeed, based on the aforementioned RG analysis of the dominance patterns of gluon-induced four-quark interaction channels [28], constraints on the EOS of isospin-symmetric QCD matter with two massless quark flavors have been computed [16]. Interestingly, the results from this study are not only consistent with EOS calculations based on chiral EFT interactions at low densities but also predict the existence of a maximum in the speed of sound at supranuclear densities which exceeds the asymptotic high-density value of the speed of sound associated with a noninteracting quark gas. The appearance of this maximum could be traced back to the formation of a diquark gap. From an astrophysical standpoint, this is worth mentioning since, at least for neutron-rich matter, the existence of a maximum in the speed of sound is presumably required to meet constraints from the analysis of neutron-star masses [13,61–64]. Recently, the fRG calculations presented in Ref. [16] have been further developed at intermediate and high densities by taking into account higher-order interactions and further resolving the momentum dependence of vertices [65]. The results from this study are consistent with those from Ref. [16]. In particular, first estimates for the speed of sound in isospin-symmetric strong-interaction matter are still found to exceed the value of the noninteracting quark gas at high densities and even increase as the density is decreased, suggesting the existence of a maximum below $n/n_0 \sim 10$, where n_0 is the nuclear saturation density.

The present work should be viewed as the first extension of our series of studies of dense strong-interaction matter [16,28,66–68] to finite isospin asymmetry, which is ultimately required to reach out to astrophysical applications. In the following, however, we do not aim at a first-principles fRG study of dense isospin-asymmetric QCD matter but at a further development of existing low-energy models for QCD with two (massless) quark flavors at intermediate and high densities by taking into account constraints from calculations based on the fundamental quark and gluon degrees of freedom [16,65]; see Sec. II. Note that, although effects from strange quarks may become relevant at high densities (see Ref. [69] for a detailed discussion), we shall ignore them in the following for simplicity. Moreover, we shall restrict ourselves to the zero-temperature limit. Nevertheless, our present work may still provide valuable information on the properties of dense QCD matter and also define a starting point for the inclusion of strange quarks in the future. The QCD-constrained low-energy model introduced in Sec. II is used in two ways in Sec. III. In Sec. III A, we employ it to estimate the zero-temperature phase diagram of asymmetric QCD matter for $n/n_0 \gtrsim 10$. Based on these results, we then discuss implications for neutron-star matter in Sec. III B by taking into account β equilibrium, electric charge neutrality, and color neutrality. In particular, we present estimates for the speed of sound. Our conclusions can be found in Sec. IV.

II. MODEL

In this section, we construct a low-energy model for QCD at intermediate and high densities by exploiting results from RG studies of the quark-gluon dynamics in this density regime [16,65]. In Sec. II A, we first discuss general aspects of our model and how it emerges from quark-gluon interactions in QCD. The effective potential of this model is then derived in Sec. II B. In Sec. II C, we present a qualitative discussion of the phase structure and the thermodynamic properties of our model, including possible implications for the properties of dense QCD matter. For more quantitative studies, it is required to determine the model parameters. In Sec. II D, we discuss how these parameters can be constrained with information from RG flows in QCD.

A. General aspects

In QCD, all interaction channels are originally generated by the quark-gluon vertex. Whereas the dynamics at high energies can be well described in a perturbative setting, the low-energy regime is governed by nonperturbative phenomena, such as spontaneous symmetry breaking. Therefore, the description of the low-energy regime by means of suitably chosen effective degrees of freedom may be efficient to capture the most relevant dynamics of QCD for a given range of the external parameters (e.g., temperature and density). For example, QCD at low densities and temperatures can be well described by means of pions and nucleons. At high densities, the dynamics in the long-range limit may then be governed by diquarks. The transformation of the effective action of QCD under a variation of the resolution and the dynamical emergence of effective degrees of freedom can be studied with RG methods [16,65,70–81].

A change in the relevant (effective) degrees of freedom suggests introducing a scale Λ_{LEM} below which a description of QCD by means of a low-energy model (LEM) constructed from a specific set of effective degrees of freedom is suitable. The actual value of Λ_{LEM} is of minor importance as it is a scheme-dependent quantity. Only the existence of this scale matters. Within a given range of external parameters, where the QCD ground state is expected to be governed by spontaneous symmetry breaking, the associated symmetry breaking (SB) scale k_{SB} may be considered a suitable estimate for Λ_{LEM}. However, the scale k_{SB} is *a priori* unknown. Even more, this choice may be impractical, as the symmetry breaking scale k_{SB} may come with an unknown dependence on the external parameters of interest. Therefore, the model scale Λ_{LEM} is

usually chosen such that spontaneous symmetry breaking has not yet set in at this scale and, at the same time, the contributions of the gauge degrees of freedom to the couplings of the low-energy model become subdominant. Such a range of scales may indeed exist. In Refs. [16,82–84], for example, it is discussed that four-quark self-interactions generated via two-gluon exchange can become strong enough to contribute as relevant operators to the RG flow. Once this is the case, the corresponding four-quark couplings $\bar{\lambda}_i$ are found to increase rapidly, indicating the onset of spontaneous symmetry breaking; see Ref. [84] for a detailed discussion.

An analysis of the RG flow of gluon-induced four-quark interactions above and close to the symmetry breaking scale k_{SB} can indeed be very useful to gain an insight into the QCD phase structure and also to identify symmetry breaking patterns which potentially govern the dynamics at low energies [28]. However, a computation of, e.g., thermodynamic observables requires us to resolve the momentum dependence of correlation functions below the symmetry breaking scale. To gain access to such observables at densities $n/n_0 \gtrsim 10$, we now construct a suitable low-energy model. To this end, we first note that a recent RG study of gluon-induced four-quark interactions suggests that the diquark channel $\sim(\bar{\psi}_b\tau_2\epsilon_{abc}\gamma_5\mathcal{C}\bar{\psi}_c^T)(\psi_d^T\mathcal{C}\gamma_5\tau_2\epsilon_{ade}\psi_e)$ is the most dominant channel in this density regime, indicating that the formation of a chirally symmetric diquark condensate $\langle\bar{\psi}_b\tau_2\epsilon_{abc}\gamma_5\mathcal{C}\bar{\psi}_c^T\rangle$ associated with pairing of the 2SC type is favored [28].[1] We therefore include this four-quark channel in the action S_{LEM} of our low-energy model, in accordance with early studies of dense strong-interaction matter [29,30,32,34–36]. Moreover, to resolve (at least some of) the momentum dependence of this channel, we shall immediately rewrite it by introducing auxiliary fields $\bar{\Delta}_a \sim (\bar{\psi}_b\tau_2\epsilon_{abc}\gamma_5\mathcal{C}\bar{\psi}_c^T)$:

$$\frac{1}{2}\mathrm{i}(\psi_b^T\mathcal{C}\gamma_5\tau_2\bar{\Delta}_a\epsilon_{abc}\psi_c) - \frac{1}{2}\mathrm{i}(\bar{\psi}_b\gamma_5\tau_2\bar{\Delta}_a^*\epsilon_{abc}\mathcal{C}\bar{\psi}_c^T) + \frac{1}{2}\bar{\lambda}_{\mathrm{csc}}^{-1}\bar{\Delta}_a^*\bar{\Delta}_a. \tag{1}$$

The four-quark coupling $\bar{\lambda}_{\mathrm{csc}}$ associated with the original four-quark channel then appears as part of the coefficient of the curvature term $\sim\bar{\Delta}_a^*\bar{\Delta}_a$. Note that, in Eq. (1), we have absorbed the Yukawa coupling $\bar{h}$ into the (auxiliary) fields $\bar{\Delta}_a = \bar{h}\Delta_a$. This implies that a finite expectation value of the complex-valued field $\bar{\Delta}_a$ can be identified with the gap in the fermionic excitation spectrum, which indicates the formation of a color superconductor.

At first glance, quark self-interaction channels of higher order may be considered parametrically suppressed at high momentum scales. For example, eight-quark interactions scale as $\sim g^8$, whereas the aforementioned four-quark interactions only scale as $\sim g^4$. Here, g denotes the strong coupling. In Ref. [65], however, it has been found that, e.g., diquarklike eight-quark interactions already become relevant above the symmetry breaking scale k_{SB}, i.e., at scales of the order of the model scale Λ_{LEM}. Therefore, a corresponding channel should also be included in the (classical) action S_{LEM} of our low-energy model. As discussed in Ref. [65], this can be conveniently done in the form of a four-diquark channel,

$$\sim\bar{\lambda}_{\mathrm{eff}}(\bar{\Delta}_a^*\bar{\Delta}_a)^2, \tag{2}$$

where $\bar{\lambda}_{\mathrm{eff}} > 0$ is an effective coupling constant. In fact, as the curvature term $\sim\bar{\Delta}_a^*\bar{\Delta}_a$, this quartic term directly affects the position of the minimum of the effective potential. Indeed, the associated eight-quark interactions lead to a weaker dependence of the gap on the chemical potential; see Ref. [65].

In principle, one may now argue that gluon-induced quark self-interactions of even higher order [e.g., as parametrized in the form of diquark interaction channels $\sim(\bar{\Delta}_a^*\bar{\Delta}_a)^{2m}$ with $m > 2$] could also become relevant at scales of the order of the model scale Λ_{LEM}, although such interactions naively scale as $\sim g^{4m}$ at high momentum scales. However, no constraints are presently available for such higher-order interactions. Therefore, we do not include them in the (classical) action S_{LEM} of our model but only take those into account for which constraints are available in Ref. [65]; see also Sec. II D.

To provide at least potentially useful information for astrophysical applications (e.g., estimates for the density dependence of thermodynamic quantities), it is required to study matter away from the isospin-symmetric limit. In our model, this is achieved by allowing for a difference in the chemical potentials of the up and down quarks. We shall refer to these flavor chemical potentials as μ_{u} and μ_{d}, respectively. With respect to studies of neutron-star matter, it is also required to implement β equilibrium which entails the inclusion of a (relativistic) kinetic term for electrons and a corresponding chemical potential μ_{e}. However, we shall neglect quark-electron interactions and interactions among the electrons themselves, as such interactions are much weaker than those governed by the strong interaction.

Our low-energy model constructed from the interaction channels (1) and (2) is not confining. While this may not be an issue at high densities, an implementation of color neutrality (not to be confused with color confinement) is nevertheless required since, e.g., neutron stars should not carry a net color charge. As detailed in Refs. [69,85,86], we shall implement color neutrality with the aid of two additional chemical potentials, μ_3 and μ_8, coupled to the color charges associated with the generators $T_3 = \lambda_3/2$ and

[1] Here, we have $\mathcal{C} = \mathrm{i}\gamma_2\gamma_0$, and the Pauli matrix τ_2 is implicitly coupled to the flavor indices of the quarks. In color space, it is summed over the totally antisymmetric tensor ϵ_{abc}.

$T_8 = \lambda_8/2$, which span the Cartan subalgebra of $\mathfrak{su}(3)$; the λ_a's are the Gell-Mann matrices.

Finally, we note that the fields $\bar{\Delta}_a$ enter our model as auxiliary fields in the spirit of a Hubbard-Stratonovich transformation [87,88]; i.e., they enter the (classical) action S_{LEM} of our model without a kinetic term. Thus, these fields are not considered to be dynamical degrees of freedom at the model scale Λ_{LEM}. Nevertheless, quantum corrections may render them dynamical. In the following, we shall ignore such corrections; see also Ref. [65] for a detailed discussion of this aspect.

B. Effective potential

Guided by the considerations in the preceding subsection, we make the following ansatz for the action of our low-energy model:

$$S_{\mathrm{LEM}} = \int \mathrm{d}^4x \Big\{ \bar{\psi}(\mathrm{i}\partial\!\!\!/ - \mathrm{i}(\hat{\mu}_{(\mathrm{f})} + \hat{\mu}_{(\mathrm{c})}))\psi + \frac{1}{2}\bar{\lambda}_{\mathrm{csc}}^{-1}\bar{\Delta}_a^*\bar{\Delta}_a + \bar{\lambda}_{\mathrm{eff}}(\bar{\Delta}_a^*\bar{\Delta}_a)^2 + \frac{1}{2}\mathrm{i}(\psi_b^T\mathcal{C}\gamma_5\tau_2\bar{\Delta}_a\epsilon_{abc}\psi_c) - \frac{1}{2}\mathrm{i}(\bar{\psi}_b\gamma_5\tau_2\bar{\Delta}_a^*\epsilon_{abc}\mathcal{C}\bar{\psi}_c^T) + \bar{\psi}^{(\mathrm{e})}(\mathrm{i}\partial\!\!\!/ - \mathrm{i}\mu_{\mathrm{e}}\gamma_0)\psi^{(\mathrm{e})} \Big\}. \tag{3}$$

Here, the fields ψ are associated with quarks whereas the fields $\psi^{(\mathrm{e})}$ describe electrons. Explicit indices of quark fields refer to their color components. For convenience, we have introduced the auxiliary operators

$$\hat{\mu}_{(\mathrm{f})} = \mathrm{diag}(\mu_{\mathrm{u}}, \mu_{\mathrm{d}})_{\mathrm{f}} \otimes \mathbb{1}_{\mathrm{c}} \otimes \gamma_0 \tag{4}$$

and

$$\hat{\mu}_{(\mathrm{c})} = \mathbb{1}_{\mathrm{f}} \otimes \mathrm{diag}(\mu_{\mathrm{r}}, \mu_{\mathrm{g}}, \mu_{\mathrm{b}})_{\mathrm{c}} \otimes \gamma_0, \tag{5}$$

where, on the right-hand side, the index f refers to flavor space and c refers to color space. The chemical potentials μ_{r}, μ_{g}, and μ_{b} associated with the three color charges (red, green, and blue) are directly related to the aforementioned chemical potentials μ_3 and μ_8. Indeed, we have

$$\mathrm{diag}(\mu_{\mathrm{r}}, \mu_{\mathrm{g}}, \mu_{\mathrm{b}})_{\mathrm{c}} = (\mu_3 T_3 + \mu_8 T_8) \tag{6}$$

with

$$\mu_{\mathrm{r}} = \frac{1}{2\sqrt{3}}\mu_8 + \frac{1}{2}\mu_3, \tag{7}$$

$$\mu_{\mathrm{g}} = \frac{1}{2\sqrt{3}}\mu_8 - \frac{1}{2}\mu_3, \tag{8}$$

$$\mu_{\mathrm{b}} = -\frac{1}{\sqrt{3}}\mu_8. \tag{9}$$

With respect to the implementation of β equilibrium, electric charge neutrality, and color neutrality, we add that the chemical potentials μ_{u}, μ_{d}, μ_3, μ_8, and μ_{e} are not independent parameters. We shall come back to this issue in Sec. III B.

Next, we compute the effective potential U of our low-energy model in a one-loop approximation where we only take into account "pure" fermion loops. To this end, we expand the auxiliary fields in Eq. (3) about a homogeneous background, which we choose to point into the 3-direction in color space for convenience. By integrating out the quarks and the electrons, we then obtain

$$U = \frac{1}{2}\bar{\lambda}_{\mathrm{csc}}^{-1}|\bar{\Delta}|^2 + \bar{\lambda}_{\mathrm{eff}}|\bar{\Delta}|^4 - \frac{\mu_{\mathrm{e}}^4}{12\pi^2} - \frac{\mu_{\mathrm{u,b}}^4}{12\pi^2} - \frac{\mu_{\mathrm{d,b}}^4}{12\pi^2} - 8\bar{l}(|\bar{\Delta}|^2) + \theta(\delta\mu^2 - |\bar{\Delta}|^2)\delta\bar{l}(|\bar{\Delta}|^2). \tag{10}$$

Here, $|\bar{\Delta}|^2 = \bar{\Delta}_3^*\bar{\Delta}_3$,[2] where $\bar{\Delta}_3$ now represents the homogeneous background field. From a minimization of U with respect to $|\bar{\Delta}|^2$, we eventually obtain the gap $\bar{\Delta}_{\mathrm{gap}}$ in the excitation spectrum of the quarks.

The contributions of the quark loops to the effective potential U depend on $|\bar{\Delta}|^2$ and are parametrized by the functions $\bar{l}$ and $\delta\bar{l}$:

$$\bar{l}(|\bar{\Delta}|^2) = \frac{1}{4\pi^2}\int_0^\Lambda \mathrm{d}p\, p^2 \Big\{ ((p+\bar{\mu})^2 + |\bar{\Delta}|^2)^{\frac{1}{2}} + ((p-\bar{\mu})^2 + |\bar{\Delta}|^2)^{\frac{1}{2}} \Big\} - \frac{1}{2\pi^2}\int_{\Lambda_{\mathrm{LEM}}}^\Lambda \mathrm{d}p\, p^2 \Big\{ (p^2 + |\bar{\Delta}|^2)^{\frac{1}{2}} + \frac{\bar{\mu}^2|\bar{\Delta}|^2}{2(p^2+|\bar{\Delta}|^2)^{\frac{3}{2}}} \Big\} \tag{11}$$

and

$$\delta\bar{l}(|\bar{\Delta}|^2) = \frac{2}{\pi^2}\int_{p_-}^{p_+} \mathrm{d}p\, p^2 \Big(\sqrt{(p-\bar{\mu})^2 + |\bar{\Delta}|^2} - |\delta\mu| \Big), \tag{12}$$

where

$$p_\pm = \bar{\mu} \pm \sqrt{\delta\mu^2 - |\bar{\Delta}|^2}. \tag{13}$$

[2]Physical observables depend only on the (gauge-invariant) quantity $|\bar{\Delta}|^2 \equiv \bar{\Delta}_a^*\bar{\Delta}_a$ (where summation over a is assumed, $a = 1, 2, 3$). Hence, they do not depend on the chosen direction of the background field in color space, see also Ref. [41]. Moreover, the invariance of the action S_{LEM} under color transformations also implies that the effective potential can only be a function of $|\bar{\Delta}|^2$. We have only picked the 3-direction for convenience which, loosely speaking, implies that the (diquark) condensate is only formed out of "red and green quarks."

We observe that $\delta\bar{l}$ does not depend on the regularization scale Λ at all. The Λ dependence of $\bar{l}$ is removed in the limit $\Lambda \to \infty$. Thus, the effective potential U does also not depend on Λ for $\Lambda \to \infty$, as it should be (see Ref. [67] for a detailed discussion). In practice, we ensure the independence of Λ by choosing sufficiently large values for Λ, i.e., $\Lambda \gg \Lambda_{\mathrm{LEM}} > \bar{\mu}$. Note that the actual representations of the functions $\bar{l}$ and $\delta\bar{l}$ depend on the details of the regularization. In the present work, we employ a three-dimensional sharp cutoff/regulator for convenience. However, our results for physical observables do not depend on the regulator, provided that the counterterms in the third and fourth lines of Eq. (11) are chosen carefully. The regulator indeed only affects scheme-dependent quantities, such as the values of the model parameters $\bar{\lambda}_{\mathrm{csc}}$ and $\bar{\lambda}_{\mathrm{eff}}$. We add that we simply employ the counterterms derived in Refs. [65,67] since these terms are not affected by the isospin asymmetry.

Let us now discuss the dependence of the effective potential U on the various chemical potentials appearing in our model. The contribution $\sim\mu_{\mathrm{e}}^4$ in the effective potential U originates from the electrons which only provide a "charged background" for $\mu_{\mathrm{e}} \neq 0$ but do not interact with the quarks otherwise.

The various quark chemical potentials enter the effective potential U only in specific combinations. To be precise, we have

$$\bar{\mu} = \frac{\mu_{\mathrm{u}} + \mu_{\mathrm{d}}}{2} + \frac{1}{2\sqrt{3}}\mu_8, \qquad \delta\mu = \frac{\mu_{\mathrm{u}} - \mu_{\mathrm{d}}}{2}. \tag{14}$$

The quantity $\bar{\mu}$ may be viewed as the average chemical potential of the two quark flavors. The isospin asymmetry can be controlled by the parameter $\delta\mu$. The chemical potential μ_3 has already been set to zero in the effective potential U. Note that this is not an additional approximation but the correct choice to ensure color neutrality in our studies of neutron-star matter; see Appendix A.

In our derivation of the effective potential U, we have chosen the background field $\bar{\Delta}_a$ to point into the 3-direction in color space for convenience. Therefore, the "blue quarks" only appear as "noninteracting spectators" in the effective potential U via their chemical potentials $\mu_{\mathrm{u,b}}$ and $\mu_{\mathrm{d,b}}$:

$$\mu_{\mathrm{u,b}} = \mu_{\mathrm{u}} - \frac{1}{\sqrt{3}}\mu_8, \qquad \mu_{\mathrm{d,b}} = \mu_{\mathrm{d}} - \frac{1}{\sqrt{3}}\mu_8. \tag{15}$$

We close this subsection by summarizing a few general aspects on the computation of thermodynamic quantities. First of all, for a given set of chemical potentials, $\vec{\mu} \coloneqq (\bar{\mu}, \delta\mu, \mu_3, \mu_8, \mu_{\mathrm{e}})$, the pressure P is obtained by evaluating the effective potential U at its minimum $|\bar{\Delta}|^2 = |\bar{\Delta}_{\mathrm{gap}}|^2$:

$$P = -U|_{\mathrm{min},\vec{\mu}} - P_0. \tag{16}$$

Here, P_0 is the *vacuum* constant (associated with $\vec{\mu} = \vec{0}$). Since the QCD vacuum is governed by spontaneous chiral symmetry breaking, this constant cannot be computed reliably within our diquark model. This entails that the pressure is also not accessible in our present study. However, toward higher densities (where diquarklike channels are expected to dominate the dynamics at low temperatures [16,28]), derivatives of the pressure with respect to the various chemical potentials are accessible. This includes densities and the speed of sound. To be specific, we have

$$n_{\mathrm{e}} = \frac{\partial P}{\partial \mu_{\mathrm{e}}} \tag{17}$$

for the electron density. The densities of the up and down quarks are given by

$$n_{\mathrm{u}} = \frac{\partial P}{\partial \mu_{\mathrm{u}}} \quad \text{and} \quad n_{\mathrm{d}} = \frac{\partial P}{\partial \mu_{\mathrm{d}}}, \tag{18}$$

respectively. Finally, the densities associated with the color charges can be obtained from

$$n_3 = \frac{\partial P}{\partial \mu_3} \quad \text{and} \quad n_8 = \frac{\partial P}{\partial \mu_8}. \tag{19}$$

At this point, we would like to add that color neutrality is ensured by choosing the chemical potentials μ_3 and μ_8 such that the "color densities" n_3 and n_8 vanish simultaneously. As discussed in Sec. III B and Appendix A, this requires us to choose $\mu_3 = 0$.

In the Introduction, we have pointed out that the speed of sound c_{s} is a quantity of particular interest in the context of astrophysical applications; see Refs. [13,61–64]. This quantity is directly related to the first derivative of the pressure with respect to the energy density ϵ,

$$c_{\mathrm{s}} = \left(\frac{\partial P}{\partial \epsilon}\right)^{\frac{1}{2}}, \tag{20}$$

where

$$\epsilon = -P + \mu_{\mathrm{u}} n_{\mathrm{u}} + \mu_{\mathrm{d}} n_{\mathrm{d}} + \mu_{\mathrm{e}} n_{\mathrm{e}}. \tag{21}$$

Note that also this quantity does not depend on the vacuum constant P_0 and is therefore accessible within our present work. In Sec. III, we shall present estimates for the speed of sound in isospin-symmetric strong-interaction matter, charge-neutral strong-interaction matter in β equilibrium, and charge- and color-neutral strong-interaction matter in β equilibrium.

C. Qualitative discussion of the phase structure and thermodynamics

Before we present numerical results for the zero-temperature phase diagram of isospin-asymmetric matter and the speed of sound, we discuss the phase structure and the thermodynamics of our model on a qualitative level. For simplicity, we shall restrict our discussion to the case of vanishing chemical potentials for the color charges throughout this subsection; i.e., we set $\mu_3 = \mu_8 = 0$. In any case, this already provides us with useful information for the determination of the parameters of our model.

Let us first consider the effective potential (10) in the isospin-symmetric case for $\bar{\mu} > 0$. We shall also assume that the parameters $\bar{\lambda}_{\rm csc}$ and $\bar{\lambda}_{\rm eff}$ have been tuned such that the loop contributions parametrized by the functions $\bar{l}$ and $\delta\bar{l}$ generate an effective potential U with a nontrivial minimum at $|\bar{\Delta}| = |\bar{\Delta}_{\rm gap}(\bar{\mu}, \delta\mu = 0)|$; see Fig. 1 (blue line) for an illustration. Note that the potential is invariant under $\delta\mu \to -\delta\mu$. Without loss of generality, it therefore suffices to consider $\delta\mu > 0$ in this subsection.

It is now important to observe that the quantum correction $\delta\bar{l}$ does not contribute to the effective potential for $\delta\mu = 0$. Even more, we deduce from Eq. (10) that an increase of the isospin-asymmetry parameter $\delta\mu$ does not affect the dependence of the effective potential on $|\bar{\Delta}|^2$ in the domain $|\bar{\Delta}|^2 > \delta\mu^2$. In particular, this implies that the position of the minimum remains unchanged for $\delta\mu^2 < |\bar{\Delta}_{\rm gap}(\bar{\mu}, \delta\mu = 0)|^2$. In other words, the original minimum of the effective potential is not shifted and remains to be a minimum for all $\delta\mu^2 < |\bar{\Delta}_{\rm gap}(\bar{\mu}, \delta\mu = 0)|^2$. However, by evaluating the effective potential, we also observe that the $\delta\mu$-dependent quark-loop contribution $\delta\bar{l}$ in Eq. (10) generates a second minimum at $|\bar{\Delta}| = 0$ for sufficiently large values of $\delta\mu$; see Fig. 1 (green line) for an illustration. These observations suggest that a critical value $\delta\mu_{\rm cr} > 0$ of the isospin-asymmetry parameter $\delta\mu$ may exist such that the minimum at $|\bar{\Delta}| = |\bar{\Delta}_{\rm gap}(\bar{\mu}, \delta\mu = 0)|$ is no longer the global minimum of the effective potential for $\delta\mu^2 > \delta\mu_{\rm cr}^2$ but may only be a local minimum, where $\delta\mu_{\rm cr}^2 < |\bar{\Delta}_{\rm gap}(\bar{\mu}, \delta\mu = 0)|^2$. At $\delta\mu = \delta\mu_{\rm cr}$, the system should then undergo a first-order phase transition. In any case, these considerations indicate the existence of a finite range of values of $\delta\mu$ for which the gap $\bar{\Delta}_{\rm gap}(\bar{\mu}, \delta\mu)$ is identical to the gap $\bar{\Delta}_{\rm gap}(\bar{\mu}, \delta\mu = 0)$ in the isospin-symmetric limit; see also Ref. [89] for a corresponding discussion.

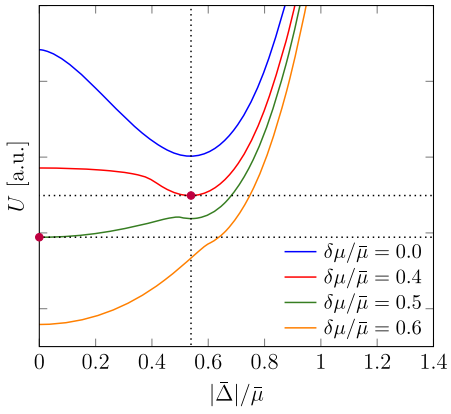

FIG. 1. Qualitative illustration of the effective potential U for $\mu_e = 0$ as a function of $|\bar{\Delta}|/\bar{\mu}$ for various values of the relative isospin asymmetry $\delta\mu/\bar{\mu}$. A discussion of the model parameters can be found in Sec. II D.

We add that not all quark degrees of freedom contribute to the formation of a color-superconducting ground state. For example, choosing the homogeneous background to point into the 3-direction in color space as done in this work, the blue quarks eventually only appear as non-interacting spectators in the effective potential; see Eq. (10). Note that, within our present approximations, a corresponding contribution to the effective potential is expected for any choice of the homogeneous background.

Let us now discuss the existence of a critical asymmetry $\delta\mu_{\rm cr}$ for the chemical potentials from a more general standpoint. The existence of such a critical value is indeed a very well-known feature of two-component Fermi gases with a superconducting ground state. For example, in the case of an electron gas, a magnetic field can be used to generate an asymmetry between "spin-up and spin-down electrons" because of the Zeeman coupling of the electron spin to the magnetic field. In other words, the magnetic field can be used to polarize the system. When the magnetic field becomes sufficiently strong, superfluidity is found to disappear, and the system undergoes a first-order phase transition to an ungapped partially polarized phase, as shown in the seminal works of Chandrasekhar [90] and Clogston [91]. This first-order phase transition is associated with a critical polarization. The search for a corresponding critical polarization in ultracold atomic two-component Fermi gases in the unitary limit has also attracted a lot of attention in the past 10–15 years; see Refs. [92–94] for reviews.

Following the works of Chandrasekhar and Clogston, the existence of a critical polarization can be understood from a comparison of the pressure of the unpolarized superfluid (gapped) phase with the pressure of the ungapped partially polarized phase. Searching for the ground state is then equivalent to searching for the phase with highest pressure (i.e., lowest Gibbs energy).

In principle, a similar line of arguments can also be applied to QCD. Loosely speaking, the formation of diquarks from quarks in the color-superconducting phase yields an energy gain per quark which is of the order of the gap $\bar{\Delta}_{\rm gap}(\bar{\mu}, \delta\mu = 0)$ in the isospin-symmetric limit. Note that the diquarks in our model are composed of one up and one down quark. Color superconductivity then disappears, if the energy $\delta\mu$ gained by adding, e.g., an up quark to the system (rather than a down quark) exceeds a critical

value $\delta\mu_{\rm cr}$. The scale for $\delta\mu_{\rm cr}$ is set by the gap $\bar{\Delta}_{\rm gap}(\bar{\mu},\delta\mu=0)$. An estimate for $\delta\mu_{\rm cr}$ can be obtained by comparing the pressure of the isospin-asymmetric quark gas in the noninteracting limit (Stefan-Boltzmann limit),

$$P_{\rm SB}(\bar{\mu},\delta\mu)=\frac{(\bar{\mu}+\delta\mu)^4}{4\pi^2}+\frac{(\bar{\mu}-\delta\mu)^4}{4\pi^2}, \tag{22}$$

with the pressure of the gapped isospin-symmetric phase evaluated at leading order in the gap [41,65,67,95,96][3]:

$$P=P_{\rm SB}(\bar{\mu},0)\left(1+2\left(\frac{\bar{\Delta}_{\rm gap}(\bar{\mu},0)}{\bar{\mu}}\right)^2+\ldots\right). \tag{23}$$

From this comparison, we obtain

$$\delta\mu_{\rm cr}(\bar{\mu})=\frac{1}{\sqrt{3}}\bar{\Delta}_{\rm gap}(\bar{\mu},0)+\ldots \tag{24}$$

for the critical isospin asymmetry.[4] We observe that $\delta\mu_{\rm cr}$ inherits the $\bar{\mu}$ dependence of the gap in the isospin-symmetric limit.[5] Moreover, since the pressure is not continuously differentiable at $\delta\mu_{\rm cr}$ for a given fixed $\bar{\mu}$, we expect the system to undergo a first-order phase transition at this point. A similar analysis for QCD with $2+1$ quark flavors can be found in Refs. [95,98].

One may now be tempted to conclude that all physical observables remain equal to their values in the isospin-symmetric limit for $\delta\mu^2<\delta\mu_{\rm cr}^2$. In particular, we may expect the pressure and the gap to remain constant within this range of values of $\delta\mu$. However, this is not the case, since, loosely speaking, only some quark degrees of freedom contribute to the formation of the color-superconducting ground state in our model; see our discussion above. The remaining other quark degrees do not couple to the (diquark) condensate. To be more specific, the formation of a finite expectation value of the form $\sim\langle\bar{\psi}_b\tau_2\epsilon_{abc}\gamma_5\mathcal{C}\bar{\psi}_c^T\rangle$ (with fixed a) is associated with the symmetry breaking pattern $\mathrm{SU}(3)\to\mathrm{SU}(2)$ in color space. For example, choosing $a=3$ for convenience (as done in all explicit calculations in the present work), a gap $\bar{\Delta}_{\rm gap}$ is only generated in the subspace of the red and green quarks. This subspace is invariant under SU(2) color transformations. The blue quarks remain ungapped. The observed independence of the gap on $\delta\mu$ below some critical value $\delta\mu_{\rm cr}$ then results from the position of the poles of the propagators of the red and green quarks in the complex p_0 plane relative to the real p_0 axis for given values of the chemical potentials, the spatial loop momentum, and the homogeneous diquark background $\bar{\Delta}_a$.[6] We emphasize that the appearance of a gap in the excitation spectrum of the quarks as well as the invariance of the gap under a shift of $\delta\mu$ (for $\delta\mu^2<\delta\mu_{\rm cr}^2$) are physical statements which may also be present in QCD although the local gauge invariance under SU(3) color transformations cannot be broken [99]. In this respect, we also add that the effective potential (10) in general depends only on the gauge-invariant quantity $\bar{\Delta}_a^*\bar{\Delta}_a$ (summation over a is assumed). These more general considerations also indicate that thermodynamic quantities (e.g., pressure and densities) should still exhibit a dependence on $\delta\mu$ for $\delta\mu^2<\delta\mu_{\rm cr}^2$ which originates from the ungapped quarks. In our numerical results for the speed of sound and the densities, we indeed observe a mild dependence on the isospin-asymmetry parameter in the gapped phase; see Sec. III B.

We close this subsection by noting that the situation encountered in the aforementioned ultracold unitary Fermi gases is slightly different. In these gases, all physical observables indeed remain equal to their values in the gapped phase up to the critical asymmetry since both fermion degrees of freedom contribute to the formation of the superconducting ground state. Note that the phase transition is found to be of first order in these gases, even if fluctuation effects are taken into account [100–103].

D. Parameter constraints from QCD

Let us begin our discussion of the determination of the model parameters $\bar{\lambda}_{\rm csc}$ and $\bar{\lambda}_{\rm eff}$ by considering the isospin-symmetric limit. In Ref. [65], an analysis of RG flows starting from the QCD action indicated that the four-quark coupling $\bar{\lambda}_{\rm csc}$ in the isospin-symmetric limit depends only very mildly on the chemical potential, at least at RG scales k (sufficiently) greater than the symmetry breaking scale $k_{\rm SB}$. Since we choose $\Lambda_{\rm LEM}>k_{\rm SB}$, we shall assume that $\bar{\lambda}_{\rm csc}$ does not depend on $\bar{\mu}$.

The situation is different for the effective four-diquark coupling $\bar{\lambda}_{\rm eff}$. Indeed, the aforementioned study of RG flows in QCD suggests that this coupling depends on the chemical potential $\bar{\mu}$, even above the symmetry breaking scale. In principle, one may now exploit the RG flows in Ref. [65] to extract the values of the couplings $\bar{\lambda}_{\rm csc}$ and $\bar{\lambda}_{\rm eff}$ at a suitably chosen model scale $\Lambda_{\rm LEM}$, which could then be used as input parameters for the evaluation of the effective potential (10) of our model. However, the values of couplings are scheme-dependent quantities, which in

[3]This expression can also be derived from Eq. (10) in the limit of vanishing four-diquark coupling. Moreover, at leading order in $\bar{\Delta}_{\rm gap}(\bar{\mu},0)/\bar{\mu}$, the general form of Eq. (23) may already be deduced from purely dimensional arguments in QCD since the gap sets the scale at high densities; see also Ref. [97] for a discussion.

[4]Here, terms of higher order in the gap have been dropped.

[5]Taking into account that effectively only two of the three color degrees of freedom of the quarks are gapped (see our discussion below), we obtain $\delta\mu_{\rm cr}(\bar{\mu})=(1/\sqrt{2})\bar{\Delta}_{\rm gap}(\bar{\mu},0)+\cdots$. This can be seen by *not* taking into account the contributions from the ungapped quarks into the analysis leading to Eq. (24).

[6]Here, p_0 refers to the zeroth component of the 4-momentum appearing in the quark propagators.

general renders such a matching of coupling values complicated. In our present work, we therefore tune the model parameters $\bar{\lambda}_{\rm csc}$ and $\bar{\lambda}_{\rm eff}$ for a given value of the chemical potential such that we recover the value of the gap found in Ref. [65]. Note that the gap in the excitation spectrum of the quarks is a physical observable.

To be specific, we choose $\Lambda_{\rm LEM} = 1$ GeV and restrict ourselves to regimes with $\bar{\mu} < \Lambda_{\rm LEM}$. For the four-quark coupling, we use $\bar{\lambda}_{\rm csc}^{-1} \approx 0.197$ GeV^2 (for all values of $\bar{\mu}$). As a function of $\bar{\mu}$, the remaining model parameter $\bar{\lambda}_{\rm eff}$ is then tuned such that the gap in our present work agrees with the one found in the study of QCD RG flows in Ref. [65]. Since the gap in this study comes with an uncertainty band originating from a variation of the RG scheme and an uncertainty in the strong coupling, we employ two parameter sets for $\bar{\lambda}_{\rm eff}$ which are associated with the lower and upper ends of the uncertainty band of the gap, respectively. The corresponding values for $\bar{\lambda}_{\rm eff}$ can be found in Ref. [65]. In Fig. 2 (green band), we show the resulting gap as a function of the baryon density n in units of the nuclear saturation density n_0.

At this point, we would like to comment on the behavior of the gap as a function of the density. In Ref. [65], a comparatively weak dependence of the gap on the chemical potential (or density) has been found; see the green-shaded band in Fig. 2. The rapid flattening of the gap with increasing density can be traced back to the emergence of the four-diquark coupling already above the symmetry breaking scale. For $n/n_0 \gtrsim 7$, the results for the gap from Ref. [65] (which we have used to fix our model parameters) are consistent with those obtained based on a Fierz-complete study of gluon-induced four-quark interaction channels [16]. This is in accordance with the fact that the latter study predicts the diquark interaction channel to be most dominant. However, for lower densities, roughly $n/n_0 \lesssim 10$, interaction channels other than the diquark channel become very relevant [28]. In particular, the chiral scalar-pseudoscalar channel starts to play a dominant role and leads to a stronger decrease of the gap than observed in Ref. [65] for decreasing density; see the red-shaded band in Fig. 2. From a comparison of the red-shaded and green-shaded band, we also cautiously conclude that the regime $n/n_0 \lesssim 7$ is no longer accessible in our present work.

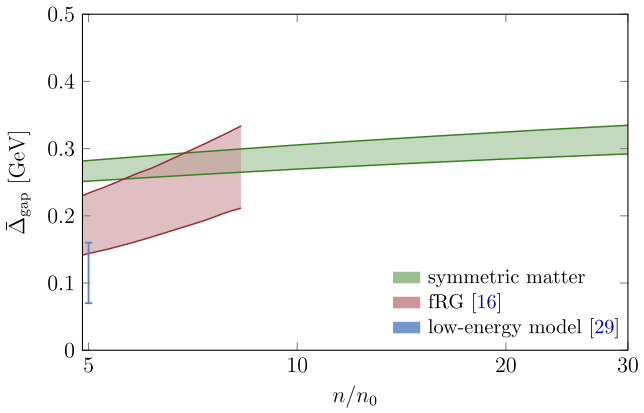

FIG. 2. Gap in the excitation spectrum of the quarks in isospin-symmetric matter as a function of the baryon density n in units of the nuclear saturation density n_0. The green-shaded band represents the gap used in the present work as input parameter (based on results from RG flows in QCD [65]). The red-shaded band depicts results from an fRG study [16]. For an example for conventional low energy model studies, we also show the result for the gap from Ref. [29].

In Fig. 2, we observe that the gap from Ref. [16] is greater than the one reported in previous low-energy model studies; see, e.g., Ref. [29]. This may be traced back to the quark-gluon dynamics underlying the study in Ref. [16]. Indeed, the quark-gluon dynamics may yield a rapid increase of the gap at lower densities, $\bar{\Delta}_{\rm gap} \sim \exp(-c/(g^4\bar{\mu}^2))$ (with $c > 0$ being a constant) [65]. Nevertheless, the results for the gap from Refs. [16,29] are still in accordance at lower densities.

Up to this point, we have basically only discussed how the parameters of our model can be fixed in the isospin-symmetric limit. However, we are aiming at studies of isospin-asymmetric strong-interaction matter. Since we use the gap to fix our model parameters, we can exploit the fact that the gap in our model is independent of the isospin-asymmetry parameter $\delta\mu$ for $\delta\mu^2 < \delta\mu_{\rm cr}^2$; see our discussion in Sec. II C and Fig. 1. For $\delta\mu^2 > \delta\mu_{\rm cr}^2$, the ground state is then described by a noninteracting isospin-asymmetric quark gas. Therefore, it is consistent to use the same model parameters for the isospin-symmetric and the isospin-asymmetric cases. Of course, the uncertainty in the isospin-symmetric gap leads to an uncertainty in our estimates for the phase structure and thermodynamics of isospin-asymmetric matter; see Sec. III. This provides insight into the sensitivity of our results for isospin-asymmetric strong-interaction matter on the uncertainty in the gap.

III. DENSE ASYMMETRIC QCD MATTER

A. Phase diagram of dense QCD matter

Since the computation of thermodynamic quantities with functional approaches also requires the computation of the order parameter, we begin our discussion of dense isospin-asymmetric strong-interaction matter by considering the zero-temperature phase diagram in the plane spanned by the total baryon density n (in units of the nuclear saturation density n_0) and the down-quark fraction $n_{\rm d}/(n_{\rm u}+n_{\rm d})$. Throughout this subsection, we shall always consider the case of vanishing color chemical potentials μ_3 and μ_8. Constraints from color neutrality are then discussed in Sec. III B.

In Fig. 3, we show the phase diagram spanned by n/n_0 and the down-quark fraction $n_{\rm d}/(n_{\rm u}+n_{\rm d})$ for $5 \leq n/n_0 \leq 30$, as obtained from an evaluation of the effective potential (10). In this phase diagram, we can identify three different

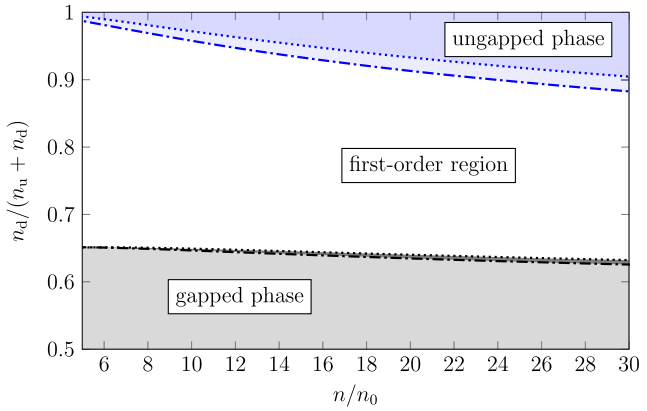

FIG. 3. Phase diagram of isospin-asymmetric strong-interaction matter in the plane spanned by the total baryon density n (in units of the nuclear saturation density n_0) and the down-quark fraction $n_d/(n_u+n_d)$. The uncertainty in the phase boundaries as depicted by different line styles results from the uncertainty in the gap (see Fig. 2), where the dotted and dot-dashed lines are associated with the upper and lower ends of the uncertainty band of the gap, respectively.

regions, a region associated with a gapped phase (gray-shaded area), a region associated with an ungapped phase (blue-shaded area), and a first-order region between these two phases. Whereas the gapped phase describes a color superconductor and is governed by spontaneous symmetry breaking, the ungapped phase can in principle be treated in a perturbative setting [52–58]. The first-order region is unstable. To be more specific, we observe that the system undergoes a (strong) first-order phase transition from the gapped phase to the ungapped phase when we increase the down-quark fraction from $n_d/(n_u+n_d)=1/2$ (symmetric matter) to $n_d/(n_u+n_d)=1$ (pure down-quark matter) for given fixed total density n/n_0.

From Fig. 3, we deduce that the phase boundaries decrease with increasing total density n/n_0. This can already be understood from a more general standpoint based on our analytic estimate of the critical asymmetry $|\delta\mu_{cr}|=|\bar{\Delta}_{gap}(\bar{\mu},\delta\mu=0)|/c_\delta+\cdots$ with $c_\delta>0$; see Eq. (24).[7] Indeed, since we have

$$\frac{n_d}{n_u+n_d}=\frac{1}{2}-\frac{3}{2}\frac{\delta\mu}{\bar{\mu}}+\ldots \tag{25}$$

for the down-quark fraction in the ungapped phase for $\delta\mu/\bar{\mu}\ll 1$, the critical down-quark fraction can be expanded as follows:

$$\left(\frac{n_d}{n_u+n_d}\right)_{cr}=\frac{1}{2}-\frac{3}{2c_\delta\bar{\mu}}\bar{\Delta}_{gap}(\bar{\mu},0)+\ldots. \tag{26}$$

Using now

$$n=\frac{1}{3}(n_u+n_d)=\frac{2\bar{\mu}^3}{3\pi^2}\left(1+3\left(\frac{\delta\mu}{\bar{\mu}}\right)^2\right) \tag{27}$$

for the total baryon density in the ungapped phase and that the gap scales as $\bar{\Delta}_{gap}\sim\exp(-c'/\bar{\mu}^2)$ with $c'>0$,[8] we find that the critical down-quark fraction scales as

$$\left(\frac{n_d}{n_u+n_d}\right)_{cr}-\frac{1}{2}\sim\frac{1}{n^{\frac{1}{3}}}\exp\left(-\frac{c''}{n^{\frac{2}{3}}}\right) \tag{28}$$

in the high-density limit, where $c''>0$ is a constant.[9] Thus, the first-order region approaches the isospin-symmetric line [i.e., $n_d/(n_u+n_d)=1/2$] for $n\to\infty$, and the extent of the gapped phase shrinks to zero in this limit. However, this does not imply that the gap along the isospin-symmetric line also tends to zero.

We add that the relation (28) for the scaling behavior of the phase boundaries is very general. In fact, we did not make use of specific properties of our model but only relied on two general assumptions: (i) the existence of a color-superconducting gap in QCD and its scaling behavior[10] and (ii) the general considerations which already led us to the scaling behavior of the critical isospin asymmetry $\delta\mu_{cr}$. For completeness, we show the analytic estimate (24) for $\delta\mu_{cr}$

[7]For our qualitative analysis in the following, only the sign of the constant c_δ matters. However, a quantitative estimate for this quantity can already be extracted from our analytic calculations above, see Eq. (24), where we have found $c_\delta=\sqrt{3}$.

[8]This is the conventional scaling behavior expected for the color-superconducting gap in (relativistic) models [29–32]. In QCD, the factor c' depends on the strong coupling g; see our discussion in Sec. II D. With respect to the gap used as input in our present study, see Fig. 2, a fit of the constant c' within the density range relevant for the present work yields $c'\approx 0.039\ \mathrm{GeV}^2$ (upper end of the green-shaded band) and $c'\approx 0.036\ \mathrm{GeV}^2$ (lower end of the green-shaded band).

[9]Here, we have used that the pressure is a continuous function of the chemical potentials, even in the presence of a first-order transition. Strictly speaking, the relation (28) describes the scaling of the upper end of the first-order region shown in Fig. 3. Since the line describing the lower end of the first-order region is bounded from above by the upper end, it is reasonable to expect that the lower end of this region exhibits a similar scaling behavior, at least at high densities.

[10]The details of the density dependence of the critical down-quark fraction in Eq. (28) are determined by the dependence of the gap on the chemical potential which may differ from the one assumed in the derivation of Eq. (28); see Refs. [31,44,46,65,104,105] for discussions of the scaling behavior of the gap in QCD. However, the statement that the phase boundaries approach the isospin-symmetric line is more general as it only relies on the assumption that $\bar{\Delta}_{gap}(\bar{\mu},0)/\bar{\mu}\to 0$ for $\bar{\mu}\to\infty$ (corresponding to $n\to\infty$). The approach to the isospin-symmetric limit may indeed be even slower than described by Eq. (28). For example, the phase boundaries may scale logarithmically as dictated by the scale dependence of the strong coupling g.

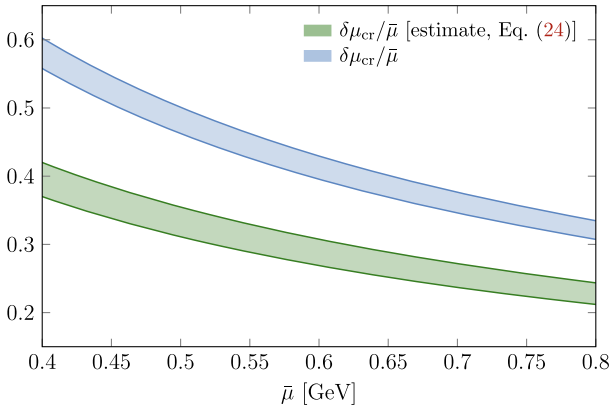

FIG. 4. Critical isospin asymmetry $\delta\mu_{\rm cr}$ (in units of $\bar{\mu}$) as a function of the average chemical potential $\bar{\mu}$. We observe that the results for this quantity obtained from a minimization of the effective potential (10) agree qualitatively with those from our analytic estimate (24).

together with the result extracted from the effective potential (10) in Fig. 4. To evaluate the analytic estimate for $\delta\mu_{\rm cr}$, we have employed the gap extracted from Eq. (10).

Specific trajectories in the phase diagram spanned by the total baryon density n and the down-quark fraction $n_{\rm d}/(n_{\rm u}+n_{\rm d})$ are of particular interest. For example, we may want to consider neutronlike matter which corresponds to the horizontal line $n_{\rm d}/(n_{\rm u}+n_{\rm d})=2/3$ in this phase diagram. From Fig. 3, we deduce that such a neutronlike matter trajectory is located in the unstable first-order region, at least within the considered density range. Toward lower densities, this trajectory may then enter the gapped phase before it finally ends up in a phase associated with spontaneous chiral symmetry breaking in the low-density regime. As discussed above, however, this low-density regime is not accessible with our present model. More importantly with respect to astrophysical applications, we shall also see in the next subsection that realistic neutron-star matter trajectories may indeed traverse the gapped phase.

B. Toward neutron-star matter

In our present work, we do not include effects from strange quarks. Nevertheless, we would like to identify trajectories in the phase diagram spanned by the total baryon density n and the down-quark fraction $n_{\rm d}/(n_{\rm u}+n_{\rm d})$ which are relevant for astrophysical applications, at least in a world with only two quark flavors. This requires us to take into account constraints from β equilibrium, electric charge neutrality, and color neutrality (not to be confused with color confinement). At least potentially, this may already provide insight into the thermodynamic properties of neutron-star matter.

Neutron-star matter is in β equilibrium; see, e.g., Refs. [69,85,95]. For our present work, this implies that there is no preferred direction for weak-interaction processes of the following type:

$$u \leftrightarrow d + e^+ + \nu_{\rm e}. \tag{29}$$

In chemical equilibrium, the chemical potentials of the particles involved in such processes are then related:

$$\mu_{\rm u} = \mu_{\rm d} + \mu_{\rm Q}. \tag{30}$$

Here, $\mu_{\rm Q}$ is the chemical potential associated with the electric charge Q, which is directly related to the electron chemical potential $\mu_{\rm e}$:

$$\mu_{\rm Q} = -\mu_{\rm e}. \tag{31}$$

In Eq. (30), we have set the chemical potential of the neutrinos $\nu_{\rm e}$ to zero since we assume that they leave the neutron star; see, e.g., Refs. [43,69,85,98,106,107] for detailed discussions of this aspect.

For a study of physical observables in β equilibrium, it is now convenient to rewrite the chemical potentials of the two quark flavors by introducing an auxiliary chemical potential μ for the quarks:

$$\mu_{\rm u} = \mu + \frac{2}{3}\mu_{\rm Q} \quad \text{and} \quad \mu_{\rm d} = \mu - \frac{1}{3}\mu_{\rm Q}. \tag{32}$$

Here, the prefactors of $\mu_{\rm Q}$ are determined by the electric charge of the up and down quarks, respectively. With these relations at hand, we can also rewrite the effective potential U. To be specific, the chemical potentials $\bar{\mu}$ and $\delta\mu$ in Eq. (10) can be expressed as a sum of the chemical potentials μ, $\mu_{\rm Q}$, and the color chemical potential μ_8:

$$\bar{\mu} = \mu + \frac{1}{6}\mu_{\rm Q} + \frac{1}{2\sqrt{3}}\mu_8 \tag{33}$$

and

$$\delta\mu = \frac{\mu_{\rm u}-\mu_{\rm d}}{2} = \frac{1}{2}\mu_{\rm Q}. \tag{34}$$

The pressure (16) then becomes a function of the chemical potentials μ, $\mu_{\rm Q}$, and μ_8. Recall that we have already set $\mu_3=0$; see below.

Electric charge neutrality can now be implemented by requiring that the charge density $n_{\rm Q}$ vanishes:

$$n_{\rm Q} = \frac{\partial P}{\partial \mu_{\rm Q}} = \frac{2}{3}n_{\rm u} - \frac{1}{3}n_{\rm d} - n_{\rm e} \overset{!}{=} 0. \tag{35}$$

In our present model, $n_{\rm e}$ is simply the density of a free relativistic electron gas, $n_{\rm e} = \mu_{\rm e}^3/(3\pi^2)$. In the phase diagram spanned by the total baryon density n and the down-quark fraction $n_{\rm d}/(n_{\rm u}+n_{\rm d})$, a trajectory respecting the constraints from β equilibrium and electric charge neutrality can be found by minimizing the effective

potential (10) with respect to $|\bar{\Delta}|^2$ for a range of values of μ, μ_Q, and μ_8 and then singling out the value of the electron chemical potential $\mu_e = -\mu_Q$ which fulfills the constraint (35) for given values of μ and μ_8. For example, considering $\mu_8 = 0$ (i.e., ignoring color neutrality), the electron chemical potential μ_e and the chemical potentials of the up and down quarks are then determined by the chemical potential μ. The total density n as well as the densities n_u and n_d are finally obtained by taking derivatives of the pressure with respect to the corresponding chemical potentials on this trajectory.

In addition to charge neutrality and β equilibrium, color neutrality should be imposed in a realistic description of neutron-star matter [69,85]. To this end, we initially included the color chemical potentials μ_3 and μ_8 in the action (3) of our model, which allow us to identify a color-neutral trajectory in the phase diagram spanned by the total baryon density n and the down-quark fraction $n_d/(n_u + n_d)$ with the aid of the following two constraints:

$$n_8 = \frac{\partial P}{\partial \mu_8} = \frac{1}{2\sqrt{3}}(n_r + n_g - 2n_b) \stackrel{!}{=} 0 \tag{36}$$

and

$$n_3 = \frac{\partial P}{\partial \mu_3} = \frac{1}{2}(n_r - n_g) \stackrel{!}{=} 0. \tag{37}$$

Here, the densities n_r, n_g, and n_b refer to the densities of the red, blue, and green quarks, respectively. We observe that $n_r = n_g = n_b$ is indeed ensured by fulfilling these two constraints.

As indicated in Sec. II B, we have already set $\mu_3 = 0$ in the effective potential U; see Eq. (10). This is not an additional approximation but follows from the constraints on n_3 and n_8 and entails that $n_3 = 0$, as detailed in Appendix A. Thus, we are left with the chemical potential μ_8, which can be determined with the aid of constraint (36).

In the plane spanned by the total density n and the down-quark fraction $n_d/(n_u + n_d)$, we can now determine a trajectory which respects the constraints from color neutrality, charge neutrality, and β equilibrium. In the following, we shall refer to this trajectory as "neutron-star matter trajectory." The computation of this trajectory requires us to simultaneously solve Eq. (35), the charge neutrality constraint, and Eq. (36), the remaining color neutrality constraint. Notably, we obtain the following exact solution for the neutron-star matter trajectory:

$$\frac{n_d}{n_u + n_d} = \frac{17}{27}. \tag{38}$$

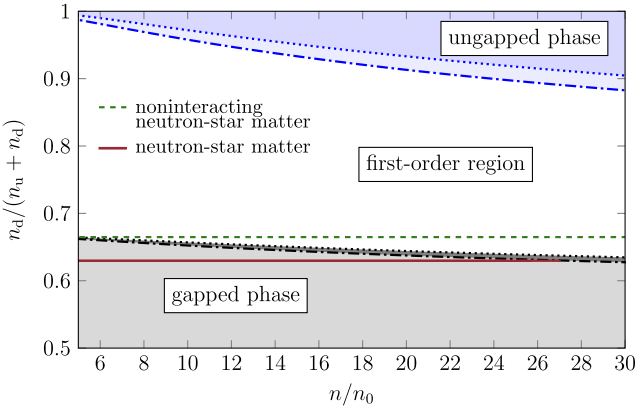

FIG. 5. Phase diagram of isospin-asymmetric strong-interaction matter spanned by the total baryon density n (in units of the nuclear saturation density n_0) and the down-quark fraction $n_d/(n_u + n_d)$. In contrast to Fig. 3, the phase boundaries now describe the points where color-neutral matter undergoes a first-order phase transition. As is the case in Fig. 3, the uncertainty in these boundaries (as depicted by different line styles) result from the uncertainty in the gap (see Fig. 2). Dotted (dot-dashed) lines are associated with the upper (lower) end of the uncertainty band of the gap. The red (solid) line depicts the neutron-star matter trajectory as obtained from our model (taking into account electric charge neutrality, β equilibrium, and color neutrality), whereas the green dashed line depicts the neutron-star matter trajectory in case of a system of noninteracting quarks.

This down-quark fraction can be translated into a ratio of protons and neutrons which are the most relevant effective degrees of freedom at low densities. We find $n_p/n_n = 1/8$, where n_n is the neutron density and n_p is the proton density. For the proton fraction $n_p/(n_p + n_n)$, we thus have $n_p/(n_p + n_n) = 1/9$, which is identical to the electron fraction: $n_e/n = n_p/(n_p + n_n) = 1/9$. Here, $n = (n_u + n_d)/3$ is the total baryon density.[11]

In Fig. 5, we show the neutron-star matter trajectory (red solid line) in the phase diagram spanned by the baryon density n and the down-quark fraction $n_d/(n_u + n_d)$. For comparison, we also show the neutron-star matter trajectory as obtained from the consideration of a noninteracting quark gas (green dashed line in Fig. 5). Note that the position of the boundaries of the gapped and ungapped phases differ slightly from those shown in Fig. 3. This difference results from the fact that the phase boundaries in Fig. 5 correspond to points where color-neutral matter undergoes a first-order transition.

[11]In contrast to most of our results, our results for the neutron-star matter trajectory and the corresponding "proton fraction" do not come with an uncertainty band. This can be traced back to the fact that terms suffering from the uncertainty in the gap cancel out in the process of solving Eqs. (35) and (36) simultaneously. If we ignore the constraint (36) from color neutrality and simply set $\mu_3 = \mu_8 = 0$, this is no longer the case; see Figs. 6 and 7.

Interestingly, we observe in Fig. 5 that the neutron-star matter trajectory traverses the gapped phase but eventually "hits" the phase boundary at $n/n_0 \gtrsim 27$. Close to the phase boundary, the gap turns out to be still sizeable within our present approximations, $\bar{\Delta}_{\rm gap}/\bar{\mu} \sim 0.3$. At the transition point, the system then undergoes a (strong) first-order phase transition from a gapped phase to an ungapped phase which may be fully accessible in a conventional perturbative setting. Note that the existence of such a phase transition may be a model-independent feature. In fact, our general considerations in Sec. III A suggest that the phase boundary of the gapped phase approaches the line associated with isospin-symmetric matter for $n \to \infty$; see Eq. (28). Thus, one may at least naively expect that neutron-star matter undergoes such a phase transition, provided that the corresponding trajectory is located within the gapped phase at some point. We emphasize that this phase transition should not be confused with a transition from a phase governed by spontaneous chiral symmetry breaking to a chirally symmetric color-superconducting (gapped) phase, which is expected to occur at much lower densities.

At this point, we also would like to add that there is no regime/"subphase" in Figs. 3 and 5 (nor in Fig. 6 to be discussed in the following), where, loosely speaking, modes with a gap in the isospin-symmetric limit are rendered gapless in the ground state by the presence of a finite isospin imbalance.[12] In particular, we observe that this type of gapless modes is not present along the neutron-star matter trajectory. The potential existence of such gapless modes in QCD matter has been discussed in detail in Refs. [109,110]; see, e.g., Refs. [43,45] for reviews.

It is instructive to investigate how color neutrality affects our results.[13] This can be done by computing the trajectory along which charge neutrality and β equilibrium are taken into account but the color-neutrality constraints are dropped (i.e., $\mu_3 = \mu_8 = 0$). In the following, we shall refer to this trajectory as "color-charged neutron-star matter trajectory." In Fig. 6, this trajectory is shown together with the (color-neutral) neutron-star matter trajectory in the plane spanned by the total density and the down-quark fraction. We find that both trajectories lie close to each other and effectively converge when the density is increased. As a consequence,

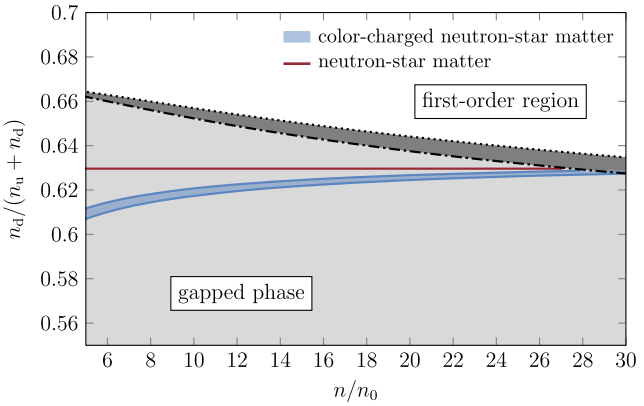

FIG. 6. Phase diagram as shown in Fig. 5 but with a reduced range of the axis associated with the down-quark fraction to show the difference between the (color-neutral) neutron-star matter trajectory (red line) and the color-charged neutron-star matter trajectory (blue band).

the electron fraction $n_{\rm e}/n$ along the color-charged neutron-star matter trajectory also approaches the one along the (color-neutral) neutron-star matter trajectory; see Fig. 7. However, toward lower densities, we observe that the electron fractions associated with the two trajectories start to deviate clearly. Recent constraints from nuclear physics and observations disfavor large electron fractions at low densities in neutron stars and also suggest that the electron fraction does not increase toward lower densities [13]. With respect to astrophysical applications, we may therefore cautiously conclude from our results that the implementation of color neutrality becomes increasingly relevant when the low-density regime is approached. In any case, the electron fractions along both trajectories are still consistent with the aforementioned constraints from nuclear physics and observations.

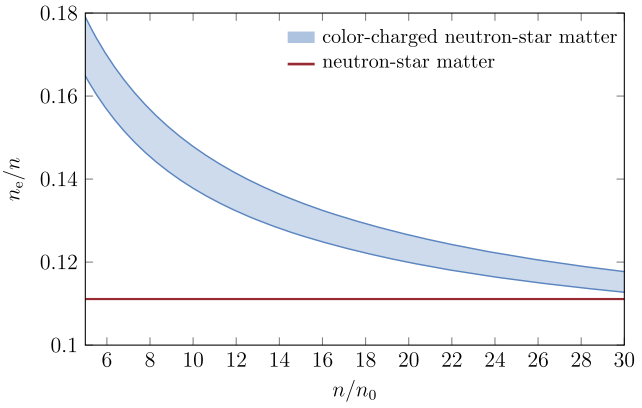

FIG. 7. Electron fraction $n_{\rm e}/n$ as a function of the total baryon density n (in units of the nuclear saturation density n_0) along the (color-neutral) neutron-star matter trajectory and the color-charged neutron-star matter trajectory. The lower (upper) end of the uncertainty band is associated with the lower (upper) end of the uncertainty band of the gap.

[12] In condensed matter physics, such a regime is referred to as the Sarma phase [108]; see, e.g., Refs. [92–94] for reviews in the context of ultracold Fermi gases.

[13] As discussed above, we expect neutron-star matter to be "color neutral" see Refs. [69,85,86,111]. Results for "color charged" neutron-star matter are shown *only* to illustrate which of the quantities considered in the present work are strongly affected by the implementation of the color-neutrality constraint, at least within our present model setup, which allows a study of both cases at comparatively low numerical costs. For numerically more intense studies of properties of strong-interaction matter, such a comparison may be potentially useful since an implementation of additional constraints (here, the color-neutrality constraint) may then be very costly from a numerical standpoint.

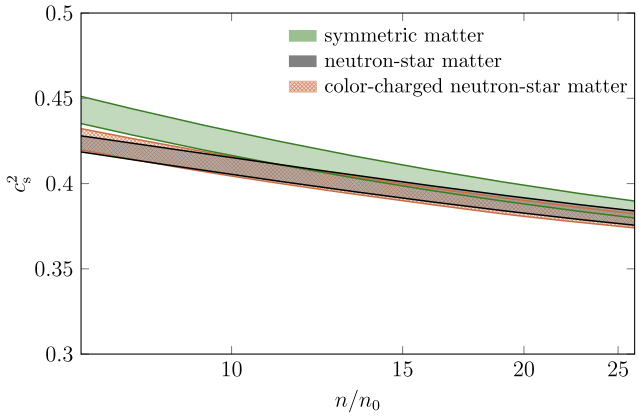

FIG. 8. Speed of sound squared (in units of the speed of light squared) in (isospin-)symmetric matter (green-shaded band), color-charged neutron-star matter (red diamond pattern), and (color-neutral) neutron-star matter (black-shaded band) as a function of the total baryon density n (from $n/n_0 = 7$ to $n/n_0 = 26$, where n_0 is the nuclear saturation density). The lower (upper) ends of the uncertainty bands are associated with the lower (upper) end of the uncertainty band of the gap.

Let us finally consider the speed of sound as another quantity of great interest with respect to astrophysical applications. To compute the speed of sound along different trajectories, we employ Eq. (20). In Fig. 8, we present our results for the speed of sound squared as a function of the total baryon density along the (color-neutral) neutron-star matter trajectory, the trajectory associated with color-charged neutron-star matter in β equilibrium, and isospin-symmetric matter (not color neutral). Note that we only show the speed of sound within the gapped phase in Fig. 8. Above $n/n_0 \gtrsim 27$, the neutron-star matter trajectory as well as the color-charged neutron-star matter trajectory cross the phase boundary; see Figs. 3 and 5. Within the gapped phase, we observe that the three trajectories lead to very similar results for the speed of sound. In particular, in all three cases, the speed of sound exceeds the value of the noninteracting quark gas and even increases toward lower densities within the considered density range. It is worth mentioning that, on a qualitative level, this behavior of the speed of sound as a function of the density can also be derived analytically from Eq. (23).[14] For example, assuming $\bar{\Delta}_{\mathrm{gap}} \sim \exp(-c'/\bar{\mu}^2)$ and $\bar{\mu} \sim n^{\frac{1}{3}}$ as in Sec. III A, we obtain the following estimate for the deviation of the speed of sound squared from its value in the noninteracting limit at high densities:

$$c_s^2 - \frac{1}{3} \sim \frac{1}{n^{\frac{2}{3}}} \exp\left(-\frac{2c''}{n^{2/3}}\right). \tag{39}$$

[14]For a detailed discussion of corrections to Eq. (23) and how they may affect the speed of sound, we refer the reader to Ref. [97].

Here, we have restricted ourselves to the isospin-symmetric case and also dropped corrections of higher order in $1/n^{1/3}$ and $(\bar{\Delta}_{\mathrm{gap}}(\bar{\mu}, 0)/\bar{\mu})$.[15] In accordance with our numerical results, we deduce from this relation that the speed of sound indeed approaches its value in the noninteracting limit from above at high densities. The latter statement appears to be insensitive to the details of our assumption for the $\bar{\mu}$ dependence of the gap. Indeed, provided that the pressure can be written in the form of Eq. (23) for small $\bar{\Delta}_{\mathrm{gap}}(\bar{\mu}, 0)/\bar{\mu}$, it is sufficient that $\bar{\Delta}_{\mathrm{gap}}(\bar{\mu}, 0)/\bar{\mu} \to 0$ for $\bar{\mu} \to \infty$ and $\bar{\Delta}_{\mathrm{gap}}(\bar{\mu}, 0)$ increases monotonically as a function of $\bar{\mu}$.

In Fig. 8, we also observe that the speed of sound along the neutron-star matter trajectory essentially agrees with the one along the color-charged neutron-star matter trajectory for the considered densities within the uncertainty bands. Recall that the electron fractions associated with these two trajectories start to deviate clearly toward lower densities; see Fig. 7. We also deduce from Fig. 8 that a finite isospin asymmetry has the tendency to slightly lower the speed of sound. However, the effect of a finite isospin asymmetry diminishes for increasing density. This does not come unexpected. In fact, our general discussion in Sec. II A already suggests that the isospin dependence may at least be weak for some observables within the color-superconducting phase. For the considered densities, this observation may provide a justification to restrict more advanced computations of thermodynamic quantities of astrophysical relevance to the isospin-symmetric limit, at least in a first step.

In Fig. 9, we finally compare our results for the speed of sound with those from a computation based on an fRG analysis of a Fierz-complete set of (gluon-induced) four-quark interactions [16]. We observe that our present results are consistent with those from Ref. [16] for $n/n_0 \gtrsim 7$. Taking also into account recent results from studies based on chiral EFT interactions at low densities [15,16], the scaling behavior of the speed of sound at high densities suggests the existence of a maximum in the speed of sound for $n/n_0 \lesssim 10$; see Fig. 9. Within the existing uncertainties, this is in accordance with the aforementioned Fierz-complete RG study starting from the QCD action [16]. Note that the existence of an increase of the speed of sound above the value associated with the noninteracting quark gas has also been observed and discussed in (low-energy)

[15]For simplicity, we have assumed that $\bar{\mu} = (\pi^2 n/2)^{1/3}$ (relation for the noninteracting quark gas). This yields the following relation between the constants c' and c'': $c'' = c'/(\pi^2/2)^{2/3}$. Of course, within the gapped phase, this is only an approximation. A more quantitative estimate may be obtained by employing an ansatz of the following form: $\bar{\mu} = c_{\bar{\mu}} n^{c_n}$, where $c_{\bar{\mu}}$ and c_n are positive constants. Thus, the actual functional dependence of the density may differ from our present estimate. Still, it appears reasonable to expect that $c_n \approx 1/3$ for large $\bar{\mu}$ where the gap becomes small compared to $\bar{\mu}$. Note also that the contribution of the ungapped "blue" quarks to the density scales as $n^{1/3}$.

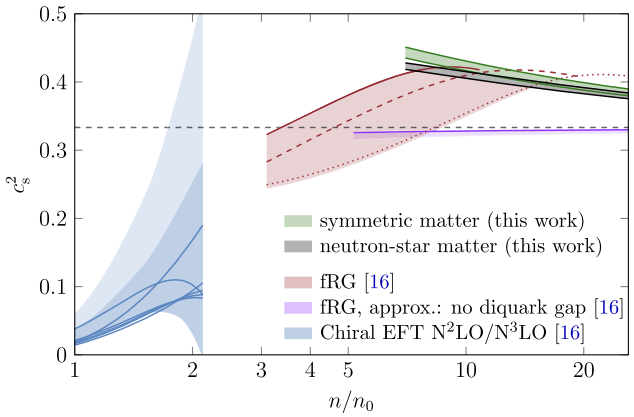

FIG. 9. Speed of sound squared (in units of the speed of light squared) in (isospin-)symmetric matter (green-shaded band, this work and Ref. [65]) and in neutron-star matter (black-shaded band, this work) as a function of n/n_0, together with results for the speed of sound in (isospin-)symmetric matter as obtained from calculations based on chiral EFT (blue-shaded bands) [16], an fRG study taking into account the formation of a diquark gap (red-shaded band) [16], and an fRG study based on an approximation without taking into account a diquark gap [16]. The black dashed line represents the speed of sound squared in a noninteracting quark gas.

models where strong-interaction matter is studied coming from low densities (see, e.g., Refs. [26,112–115]) rather than from high densities as done in the present work. Interestingly, such an increase of the speed of sound has also been observed in a recent lattice study of two-color QCD [116].

With respect to astrophysical applications, we add that constraints from neutron-star masses strongly suggest the existence of such a maximum in neutron-rich matter [13,61–64]. However, a computation of the position of this maximum is beyond the scope of the present work, as it will most likely require the inclusion of additional effective degrees of freedom, such as pions, vector mesons, and nucleons, which are expected to become relevant in this density regime [25,26,28,112,117].

Of course, another quantity of great relevance for astrophysical applications is the pressure as a function of the density. Up to a constant (vacuum constant), this quantity can be obtained by an integration of the speed of sound squared with respect to the energy density; see Eq. (20). In (low-energy) model studies, different ways of determining this constant have been discussed; see, e.g., Refs. [112–115]. In the following, we shall not determine this constant but only note that a combination of our present work with Refs. [16,65] may be used in the future to compute estimates of the pressure and the speed of sound of isospin-imbalanced strong-interaction matter by studying RG flows starting from the QCD action at high momentum scales. Results for the pressure of symmetric matter from such an RG study can be found in Ref. [16], in which also a comparison of the pressure with results from model studies is provided. Our present study of the speed of sound (see Figs. 8 and 9) suggests that the results for the pressure presented in Ref. [16] may depend only mildly on the isospin asymmetry at high densities, at least for imbalances relevant for astrophysical applications. However, a detailed analysis of this aspect is deferred to future work.

IV. CONCLUSIONS

To study the zero-temperature phase diagram of strong-interaction matter with two massless quark flavors at supranuclear densities, we have constructed a model based on constraints from studies of RG flows in QCD [16,28,65]. In this model, the dynamics is found to be governed by the formation of a color-superconducting gap at sufficiently small down-quark fractions. By increasing the down-quark fraction for a fixed total density, we have found that the system undergoes a (strong) first-order phase transition to an ungapped quark-matter phase. Our results suggest that, if this phase transition occurs in two-flavor QCD, the associated phase boundary in the phase diagram spanned by the total baryon density and the down-quark fraction approaches the isospin-symmetric line when the density is increased.

The results for the zero-temperature phase diagram of our model are in accordance with more general considerations which do not rely on specific details of our model; see our discussion in Sec. III A. These considerations already suggest that dense neutron-star matter may undergo a first-order phase transition from a color-superconducting phase to an ungapped quark matter phase. However, in terms of the density, the position of this transition to the ungapped phase may be well beyond densities relevant for astrophysical applications. Note that our analysis also indicates that isospin-symmetric strong-interaction matter does not undergo such a phase transition at high densities.

By taking into account constraints from β equilibrium, charge neutrality, and color neutrality in our model, we have determined a neutron-star matter trajectory in the phase diagram spanned by the total baryon density and the down-quark fraction. This trajectory is found to be located in the gapped phase for $n/n_0 \lesssim 27$ but "hits" the boundary of this phase toward higher densities, as suggested by our general considerations. Along this trajectory (but below the phase transition), we have computed two quantities of particular interest in the context of astrophysical applications: the electron fraction and the speed of sound. Our results for both quantities are in accordance with constraints from nuclear physics and observations [13]. In particular, we have found that the speed of sound along the neutron-star matter trajectory exceeds the asymptotic value associated with the noninteracting quark gas and even increases toward lower densities across a wide range. Taking into account results from studies based on chiral EFT interactions at low densities [15,16], the observed behavior of the speed of sound at $n/n_0 \gtrsim 10$ suggests the existence of a

maximum in this quantity at intermediate densities, as also discussed for isospin-symmetric matter in Ref. [16]. Note that constraints from neutron-star masses also strongly support the existence of a maximum in the speed of sound in neutron-rich matter [13,61–64].

With respect to astrophysical applications, it should be added that strange quarks may become relevant in the density regime considered in this work. In fact, taking strange quarks into account, the ground state associated with pairing of the two-flavor color-superconductor type (as considered in this work) may no longer be favored [69]. Still, for example, our general considerations regarding the density dependence of the speed of sound do not rely on the specific type of the gap but only on the dependence of the pressure on the gap and may therefore also hold in the presence of strange quarks, at least in case of color-flavor locking at high densities.[16] In any case, the construction of a $2+1$-flavor model based on, e.g., constraints from RG flows in QCD is in principle also possible but appears to be much more challenging. For example, the number of possible channels in a Fierz-complete analysis of gluon-induced four-quark interactions already grows drastically because of the explicit breaking of the flavor symmetry [118]. Leaving this ambitious endeavor aside, our present work may still help to gain a better understanding of the properties of dense strong-interaction matter in general.

ACKNOWLEDGMENTS

The authors would like to thank M. Buballa, J. E. Drut, A. Geißel, T. Gorda, K. Hebeler, J. M. Pawlowski, D. Rischke, and A. Schwenk for useful discussions and comments on the manuscript. As members of the fQCD Collaboration [119], the authors also would like to thank the other members of this collaboration for discussions and providing data for cross-checks. J. B. acknowledges support by the DFG under Grants No. BR 4005/4-1 and No. BR 4005/6-1 (Heisenberg program). This work is supported by the Deutsche Forschungsgemeinschaft (DFG, German Research Foundation), Project No. 279384907—SFB 1245 and by the State of Hesse within the Research Cluster ELEMENTS (Project No. 500/10.006).

APPENDIX A: COMMENT ON COLOR NEUTRALITY

In Sec. II B, we introduce the effective potential U of our model, which turns out to be independent of the color chemical potential μ_3; see Eq. (10). In this Appendix, we show that this choice for μ_3 is correct for studies of color-neutral matter. To this end, we consider the effective potential U for finite μ_3:

$$\begin{aligned} U = {} & \frac{1}{2}\bar{\lambda}_{\mathrm{csc}}^{-1}|\bar{\Delta}|^2 + \bar{\lambda}_{\mathrm{eff}}|\bar{\Delta}|^4 - \frac{\mu_{\mathrm{u,b}}^4}{12\pi^2} - \frac{\mu_{\mathrm{d,b}}^4}{12\pi^2} - \frac{\mu_{\mathrm{e}}^4}{12\pi^2} \\ & - 4\bar{l}(|\bar{\Delta}|^2)|_{\bar{\mu}=\mu_{\mathrm{rg}}} - 4\bar{l}(|\bar{\Delta}|^2)|_{\bar{\mu}=\mu_{\mathrm{gr}}} \\ & + \frac{1}{2}\theta(\delta\mu_{\mathrm{rg}}^2 - |\bar{\Delta}|^2)\delta\bar{l}(|\bar{\Delta}|^2)|_{\substack{\bar{\mu}=\mu_{\mathrm{rg}} \\ \delta\mu=\delta\mu_{\mathrm{rg}}}} \\ & + \frac{1}{2}\theta(\delta\mu_{\mathrm{gr}}^2 - |\bar{\Delta}|^2)\delta\bar{l}(|\bar{\Delta}|^2)|_{\substack{\bar{\mu}=\mu_{\mathrm{gr}} \\ \delta\mu=\delta\mu_{\mathrm{gr}}}} . \end{aligned} \tag{A1}$$

Here,

$$\delta\mu_{\mathrm{rg}} = \delta\mu + \frac{1}{2}\mu_3, \qquad \delta\mu_{\mathrm{gr}} = \delta\mu - \frac{1}{2}\mu_3 \tag{A2}$$

and

$$\begin{aligned} \mu_{\mathrm{rg}} &= \frac{\mu_{\mathrm{u}} + \mu_{\mathrm{d}}}{2} + \frac{\mu_{\mathrm{r}} + \mu_{\mathrm{g}}}{2} \\ &= \frac{\mu_{\mathrm{u}} + \mu_{\mathrm{d}}}{2} + \frac{1}{2\sqrt{3}}\mu_8 \end{aligned} \tag{A3}$$

are chemical potentials associated with red and green quarks. Note that we have

$$\mu_{\mathrm{gr}} = \mu_{\mathrm{rg}} \tag{A4}$$

and

$$\mu_3 = \mu_{\mathrm{r}} - \mu_{\mathrm{g}}. \tag{A5}$$

The chemical potentials related to blue quarks are

$$\mu_{\mathrm{u,b}} = \mu_{\mathrm{u}} + \mu_{\mathrm{b}} = \mu_{\mathrm{u}} - \frac{1}{\sqrt{3}}\mu_8 \tag{A6}$$

and

$$\mu_{\mathrm{d,b}} = \mu_{\mathrm{d}} + \mu_{\mathrm{b}} = \mu_{\mathrm{d}} - \frac{1}{\sqrt{3}}\mu_8. \tag{A7}$$

Note that, in contrast to the blue quarks, the chemical potentials of the green and red quarks do not appear explicitly in our equations as we have chosen to replace them with suitable combinations of μ_{u}, μ_{d}, μ_3, μ_8, and $\delta\mu$; see, e.g., Eq. (A3). Such a replacement is convenient since the red and green quarks "mix" in the color-superconducting phase anyhow. Finally, we add that the functions $\bar{l}$ and $\delta\bar{l}$ associated with loop integrals are given in Eqs. (11) and (12), respectively.

Strong-interaction matter is said to be color neutral (not to be confused with color confinement), if the densities of the three color charges are identical: $n_{\mathrm{r}} = n_{\mathrm{g}} = n_{\mathrm{b}}$. As discussed in Sec. II A, this can be achieved by requiring that the densities n_3 and n_8 (associated with the color chemical potentials μ_3 and μ_8) vanish:

[16] We refer to Appendix B for a comment on this aspect.

$$n_8 = \frac{\partial P}{\partial \mu_8} = \frac{1}{2\sqrt{3}}\frac{\partial P}{\partial \mu_r} + \frac{1}{2\sqrt{3}}\frac{\partial P}{\partial \mu_g} - \frac{1}{\sqrt{3}}\frac{\partial P}{\partial \mu_b} = \frac{1}{2\sqrt{3}}(n_r + n_g - 2n_b) \stackrel{!}{=} 0 \quad \text{(A8)}$$

and

$$n_3 = \frac{\partial P}{\partial \mu_3} = \frac{1}{2}\frac{\partial P}{\partial \mu_r} - \frac{1}{2}\frac{\partial P}{\partial \mu_g} = \frac{1}{2}(n_r - n_g) \stackrel{!}{=} 0. \quad \text{(A9)}$$

Since the effective potential (A1) is invariant under r $\leftrightarrow$ g, we have $P(\mu_r, \mu_g) = P(\mu_g, \mu_r)$. Thus, the constraint (A9) is fulfilled, if $\mu_r = \mu_g$, which is equivalent to $\mu_3 = 0$. For the purposes of the present work, it is therefore justified to set $\mu_3 = 0$ in the effective potential U, as done in Eq. (10).

APPENDIX B: COMMENT ON STRANGE-QUARK EFFECTS

Considering the case of two massless quark flavors plus a strange quark with mass m_s, it has been shown in Ref. [69] (see also Ref. [46] for a review) that, to order m_s^4 and second order in the gap, the pressure for color-flavor locked (CFL) quark matter can be written as

$$P_{\mathrm{CFL}} = P_{\mathrm{CFL}}^{(0)}(\mu, m_s) + c_\Delta(\bar{\Delta}_{\mathrm{gap}}^{\mathrm{CFL}})^2\mu^2 + \ldots, \quad \text{(B1)}$$

where $\bar{\Delta}_{\mathrm{gap}}^{\mathrm{CFL}}$ is the CFL gap, $P_{\mathrm{CFL}}^{(0)}$ is the pressure of unpaired quark matter including terms depending explicitly on the strange quark mass, and c_Δ is a positive constant. Note that we tacitly assume that the gap divided by the chemical potential is sufficiently large, measured relative to $(m_s/\mu)^2$, such that the CFL phase is favored over unpaired quark matter [69]. Moreover, as done in Ref. [69], we have dropped the leading-order strange-quark mass correction $\sim m_s^2/\mu^2$ to the CFL gap.

At least at high densities, where the leading-order expression (B1) may be expected to be valid, it follows that the dependence of the pressure on the gap in the CFL phase is qualitatively the same as in the case of strong-interaction matter with only two massless quark flavors; see Eq. (23). Assuming now that the CFL gap exhibits the typical Bardeen-Cooper-Schrieffer (BCS)-type dependence on the chemical potential and that $\bar{\Delta}_{\mathrm{gap}}^{\mathrm{CFL}}(\mu)/\mu \to 0$ for $\mu \to \infty$ (as it is the case for the 2SC gap), we cautiously conclude that the speed of sound in the CFL phase also exceeds the asymptotic value $c_s = 1/\sqrt{3}$ and exhibits a density dependence similar to the one in Eq. (39), at least at sufficiently high densities. Recall that the density dependence of the speed of sound given in Eq. (39) follows from the expansion (23) for the pressure.

[1] B. P. Abbott *et al.* (LIGO Scientific and Virgo Collaborations), Phys. Rev. Lett. **119**, 161101 (2017).
[2] B. P. Abbott *et al.* (LIGO Scientific and Virgo Collaborations), Phys. Rev. X **9**, 011001 (2019).
[3] A. L. Watts *et al.*, Rev. Mod. Phys. **88**, 021001 (2016).
[4] Z. Arzoumanian *et al.*, Proc. SPIE Int. Soc. Opt. Eng. **9144**, 914420 (2014).
[5] K. C. Gendreau *et al.*, Proc. SPIE Int. Soc. Opt. Eng. **9905**, 99051H (2016).
[6] M. C. Miller *et al.*, Astrophys. J. Lett. **918**, L28 (2021).
[7] T. E. Riley *et al.*, Astrophys. J. Lett. **918**, L27 (2021).
[8] G. Raaijmakers, S. K. Greif, K. Hebeler, T. Hinderer, S. Nissanke, A. Schwenk, T. E. Riley, A. L. Watts, J. M. Lattimer, and W. C. G. Ho, Astrophys. J. Lett. **918**, L29 (2021).
[9] P. Demorest, T. Pennucci, S. Ransom, M. Roberts, and J. Hessels, Nature (London) **467**, 1081 (2010).
[10] J. Antoniadis *et al.*, Science **340**, 448 (2013).
[11] E. Fonseca *et al.*, Astrophys. J. **832**, 167 (2016).
[12] H. T. Cromartie *et al.*, Nat. Astron. **4**, 72 (2020).
[13] S. Huth, C. Wellenhofer, and A. Schwenk, Phys. Rev. C **103**, 025803 (2021).
[14] E. Epelbaum, H.-W. Hammer, and U.-G. Meissner, Rev. Mod. Phys. **81**, 1773 (2009).
[15] K. Hebeler, J. M. Lattimer, C. J. Pethick, and A. Schwenk, Astrophys. J. **773**, 11 (2013).
[16] M. Leonhardt, M. Pospiech, B. Schallmo, J. Braun, C. Drischler, K. Hebeler, and A. Schwenk, Phys. Rev. Lett. **125**, 142502 (2020).
[17] K. Hebeler, Phys. Rep. **890**, 1 (2021).
[18] J. Berges, D. U. Jungnickel, and C. Wetterich, Int. J. Mod. Phys. A **18**, 3189 (2003).
[19] K. Kamikado, N. Strodthoff, L. von Smekal, and J. Wambach, Phys. Lett. B **718**, 1044 (2013).
[20] M. Drews and W. Weise, Phys. Lett. B **738**, 187 (2014).
[21] M. Drews and W. Weise, Phys. Rev. C **91**, 035802 (2015).
[22] R.-A. Tripolt, B.-J. Schaefer, L. von Smekal, and J. Wambach, Phys. Rev. D **97**, 034022 (2018).
[23] K. Otto, M. Oertel, and B.-J. Schaefer, Phys. Rev. D **101**, 103021 (2020).
[24] K. Otto, M. Oertel, and B.-J. Schaefer, Eur. Phys. J. Spec. Top. **229**, 3629 (2020).
[25] Y. Song, G. Baym, T. Hatsuda, and T. Kojo, Phys. Rev. D **100**, 034018 (2019).
[26] R. D. Pisarski, Phys. Rev. D **103**, L071504 (2021).
[27] R.-A. Tripolt, C. Jung, L. von Smekal, and J. Wambach, Phys. Rev. D **104**, 054005 (2021).

[28] J. Braun, M. Leonhardt, and M. Pospiech, Phys. Rev. D **101**, 036004 (2020).
[29] M. G. Alford, K. Rajagopal, and F. Wilczek, Phys. Lett. B **422**, 247 (1998).
[30] R. Rapp, T. Schäfer, E. V. Shuryak, and M. Velkovsky, Phys. Rev. Lett. **81**, 53 (1998).
[31] T. Schäfer and F. Wilczek, Phys. Lett. B **450**, 325 (1999).
[32] J. Berges and K. Rajagopal, Nucl. Phys. **B538**, 215 (1999).
[33] D. T. Son, Phys. Rev. D **59**, 094019 (1999).
[34] T. Schäfer and F. Wilczek, Phys. Rev. D **60**, 114033 (1999).
[35] R. D. Pisarski and D. H. Rischke, Phys. Rev. D **61**, 051501 (2000).
[36] R. D. Pisarski and D. H. Rischke, Phys. Rev. D **61**, 074017 (2000).
[37] W. E. Brown, J. T. Liu, and H.-c. Ren, Phys. Rev. D **61**, 114012 (2000).
[38] N. J. Evans, J. Hormuzdiar, S. D. H. Hsu, and M. Schwetz, Nucl. Phys. **B581**, 391 (2000).
[39] D. K. Hong, V. A. Miransky, I. A. Shovkovy, and L. C. R. Wijewardhana, Phys. Rev. D **61**, 056001 (2000); **62**, 059903(E) (2000).
[40] D. Bailin and A. Love, Phys. Rep. **107**, 325 (1984).
[41] K. Rajagopal and F. Wilczek, The condensed matter physics of QCD, in *At the Frontier of Particle Physics. Handbook of QCD. Vol. 1-3*, edited by M. Shifman and B. Ioffe (World Scientific, Singapore, 2000), pp. 2061–2151.
[42] M. G. Alford, Annu. Rev. Nucl. Part. Sci. **51**, 131 (2001).
[43] M. Buballa, Phys. Rep. **407**, 205 (2005).
[44] D. H. Rischke, Prog. Part. Nucl. Phys. **52**, 197 (2004).
[45] I. A. Shovkovy, Found. Phys. **35**, 1309 (2005).
[46] M. G. Alford, A. Schmitt, K. Rajagopal, and T. Schäfer, Rev. Mod. Phys. **80**, 1455 (2008).
[47] K. Fukushima and T. Hatsuda, Rep. Prog. Phys. **74**, 014001 (2011).
[48] K. Fukushima, J. Phys. G **39**, 013101 (2012).
[49] R. Anglani, R. Casalbuoni, M. Ciminale, N. Ippolito, R. Gatto, M. Mannarelli, and M. Ruggieri, Rev. Mod. Phys. **86**, 509 (2014).
[50] A. Schmitt, *Introduction to Superfluidity: Field-Theoretical Approach and Applications* (Springer, New York, 2015), Vol. 888.
[51] G. Baym, T. Hatsuda, T. Kojo, P. D. Powell, Y. Song, and T. Takatsuka, Rep. Prog. Phys. **81**, 056902 (2018).
[52] B. A. Freedman and L. D. McLerran, Phys. Rev. D **16**, 1130 (1977).
[53] B. A. Freedman and L. D. McLerran, Phys. Rev. D **16**, 1169 (1977).
[54] V. Baluni, Phys. Rev. D **17**, 2092 (1978).
[55] A. Kurkela, P. Romatschke, and A. Vuorinen, Phys. Rev. D **81**, 105021 (2010).
[56] E. S. Fraga, A. Kurkela, and A. Vuorinen, Astrophys. J. Lett. **781**, L25 (2014).
[57] E. S. Fraga, A. Kurkela, J. Schaffner-Bielich, and A. Vuorinen, Nucl. Phys. **A956**, 813 (2016).
[58] T. Gorda, A. Kurkela, P. Romatschke, M. Säppi, and A. Vuorinen, Phys. Rev. Lett. **121**, 202701 (2018).
[59] T. Gorda, A. Kurkela, R. Paatelainen, S. Säppi, and A. Vuorinen, Phys. Rev. Lett. **127**, 162003 (2021).
[60] T. Gorda, A. Kurkela, R. Paatelainen, S. Säppi, and A. Vuorinen, Phys. Rev. D **104**, 074015 (2021).
[61] P. Bedaque and A. W. Steiner, Phys. Rev. Lett. **114**, 031103 (2015).
[62] I. Tews, J. Carlson, S. Gandolfi, and S. Reddy, Astrophys. J. **860**, 149 (2018).
[63] S. K. Greif, G. Raaijmakers, K. Hebeler, A. Schwenk, and A. L. Watts, Mon. Not. R. Astron. Soc. **485**, 5363 (2019).
[64] E. Annala, T. Gorda, A. Kurkela, J. Nättilä, and A. Vuorinen, Nat. Phys. **16**, 907 (2020).
[65] J. Braun and B. Schallmo, Phys. Rev. D **105**, 036003 (2022).
[66] J. Braun, M. Leonhardt, and M. Pospiech, Phys. Rev. D **96**, 076003 (2017).
[67] J. Braun, M. Leonhardt, and J. M. Pawlowski, SciPost Phys. **6**, 056 (2019).
[68] J. Braun, T. Dörnfeld, B. Schallmo, and S. Töpfel, Phys. Rev. D **104**, 096002 (2021).
[69] M. Alford and K. Rajagopal, J. High Energy Phys. 06 (2002) 031.
[70] H. Gies and C. Wetterich, Phys. Rev. D **65**, 065001 (2002).
[71] H. Gies and C. Wetterich, Phys. Rev. D **69**, 025001 (2004).
[72] J. M. Pawlowski, Ann. Phys. (Amsterdam) **322**, 2831 (2007).
[73] H. Gies, Lect. Notes Phys. **852**, 287 (2012).
[74] J. Braun, Eur. Phys. J. C **64**, 459 (2009).
[75] S. Floerchinger and C. Wetterich, Phys. Lett. B **680**, 371 (2009).
[76] J. Braun, L. M. Haas, F. Marhauser, and J. M. Pawlowski, Phys. Rev. Lett. **106**, 022002 (2011).
[77] J. Braun, L. Fister, J. M. Pawlowski, and F. Rennecke, Phys. Rev. D **94**, 034016 (2016).
[78] M. Mitter, J. M. Pawlowski, and N. Strodthoff, Phys. Rev. D **91**, 054035 (2015).
[79] A. K. Cyrol, M. Mitter, J. M. Pawlowski, and N. Strodthoff, Phys. Rev. D **97**, 054006 (2018).
[80] W.-j. Fu, J. M. Pawlowski, and F. Rennecke, Phys. Rev. D **101**, 054032 (2020).
[81] K. Fukushima, J. M. Pawlowski, and N. Strodthoff, arXiv:2103.01129.
[82] J. Braun and H. Gies, Phys. Lett. B **645**, 53 (2007).
[83] J. Braun and H. Gies, J. High Energy Phys. 06 (2006) 024.
[84] J. Braun, J. Phys. G **39**, 033001 (2012).
[85] A. W. Steiner, S. Reddy, and M. Prakash, Phys. Rev. D **66**, 094007 (2002).
[86] M. Buballa and I. A. Shovkovy, Phys. Rev. D **72**, 097501 (2005).
[87] J. Hubbard, Phys. Rev. Lett. **3**, 77 (1959).
[88] R. Stratonovich, Dokl. Akad. Nauk. **115**, 1097 (1957).
[89] P. F. Bedaque, Nucl. Phys. **A697**, 569 (2002).
[90] B. S. Chandrasekhar, Appl. Phys. Lett. **1**, 7 (1962).
[91] A. M. Clogston, Phys. Rev. Lett. **9**, 266 (1962).
[92] F. Chevy and C. Mora, Rep. Prog. Phys. **73**, 112401 (2010).
[93] *The BCS-BEC Crossover and the Unitary Fermi Gas*, edited by W. Zwerger (Springer-Verlag, Berlin Heidelberg, 2012).
[94] K. Gubbels and H. Stoof, Phys. Rep. **525**, 255 (2013).
[95] K. Rajagopal and F. Wilczek, Phys. Rev. Lett. **86**, 3492 (2001).

[96] I. A. Shovkovy and P. J. Ellis, Phys. Rev. C **66**, 015802 (2002).
[97] J. Braun, A. Geißel, and B. Schallmo, arXiv:2206.06328.
[98] M. G. Alford, K. Pangeni, and A. Windisch, Phys. Rev. Lett. **120**, 082701 (2018).
[99] S. Elitzur, Phys. Rev. D **12**, 3978 (1975).
[100] I. Boettcher, J. Braun, T. K. Herbst, J. M. Pawlowski, D. Roscher, and C. Wetterich, Phys. Rev. A **91**, 013610 (2015).
[101] I. Boettcher, T. K. Herbst, J. M. Pawlowski, N. Strodthoff, L. von Smekal, and C. Wetterich, Phys. Lett. B **742**, 86 (2015).
[102] D. Roscher, J. Braun, and J. E. Drut, Phys. Rev. A **91**, 053611 (2015).
[103] B. Frank, J. Lang, and W. Zwerger, J. Exp. Theor. Phys. **127**, 812 (2018).
[104] N. J. Evans, S. D. H. Hsu, and M. Schwetz, Nucl. Phys. **B551**, 275 (1999).
[105] N. J. Evans, S. D. H. Hsu, and M. Schwetz, Phys. Lett. B **449**, 281 (1999).
[106] D. Ebert and K. G. Klimenko, Eur. Phys. J. C **46**, 771 (2006).
[107] J. O. Andersen and L. Kyllingstad, J. Phys. G **37**, 015003 (2009).
[108] G. Sarma, J. Phys. Chem. Solids **24**, 1029 (1963).
[109] I. Shovkovy and M. Huang, Phys. Lett. B **564**, 205 (2003).
[110] M. Huang and I. Shovkovy, Nucl. Phys. **A729**, 835 (2003).
[111] P. Amore, M. C. Birse, J. A. McGovern, and N. R. Walet, Phys. Rev. D **65**, 074005 (2002).
[112] L. McLerran and S. Reddy, Phys. Rev. Lett. **122**, 122701 (2019).
[113] G. A. Contrera, D. Blaschke, J. P. Carlomagno, A. G. Grunfeld, and S. Liebing, Phys. Rev. C **105**, 045808 (2022).
[114] O. Ivanytskyi and D. Blaschke, Phys. Rev. D **105**, 114042 (2022).
[115] T. Kojo, D. Hou, J. Okafor, and H. Togashi, Phys. Rev. D **104**, 063036 (2021).
[116] K. Iida and E. Itou, arXiv:2207.01253.
[117] J. Braun, M. Leonhardt, and M. Pospiech, Phys. Rev. D **97**, 076010 (2018).
[118] J. Braun, M. Leonhardt, J. M. Pawlowski, and D. Rosenblüh, arXiv:2012.06231.
[119] J. Braun, Y.-r. Chen, W.-j. Fu, F. Gao, A. Geißel, F. Ihssen, J. Horak, C. Huang, J. M. Pawlowski, F. Rennecke, F. Sattler, B. Schallmo, C. Schneider, Y.-y. Tan, S. Töpfel, R. Wen, J. Wessely, N. Wink, and S. Yin (fQCD Collaboration) (members as of March 2022).